The Journal of Chemical Physics ARTICLE scitation.org/journal/jcp

Analytic gradient for the QM/MM-Ewald method using charges derived from the electrostatic potential: Theory, implementation, and application to *ab initio* molecular dynamics simulation of the aqueous electron

Cite as: J. Chem. Phys. 150, 144115 (2019); doi: 10.1063/1.5089673
Submitted: 21 January 2019 • Accepted: 7 March 2019 •
Published Online: 9 April 2019

View Online Export Citation CrossMark

Zachary C. Holden,[a] Bhaskar Rana, and John M. Herbert[b]

AFFILIATIONS

Department of Chemistry and Biochemistry, The Ohio State University, Columbus, Ohio 43210, USA

[a]**Current address:** Department of Chemistry and Physics, Indiana State University, Terre Haute, Indiana 47809, USA.
[b]herbert@chemistry.ohio-state.edu

ABSTRACT

We report an implementation of periodic boundary conditions for mixed quantum mechanics/molecular mechanics (QM/MM) simulations, in which atomic partial charges are used to represent periodic images of the QM region. These charges are incorporated into the Fock matrix in a manner that preserves the variational nature of the self-consistent field procedure, and their interactions with the MM charges are summed using the conventional Ewald technique. To ensure that the procedure is stable in arbitrary basis sets, the atomic charges are derived by least-squares fit to the electrostatic potential generated by the QM region. We formulate and implement analytic energy gradients for the QM/MM-Ewald method and demonstrate that stable molecular dynamics simulations are thereby obtained. As a proof-of-concept application, we perform QM/MM simulations of a hydrated electron in bulk liquid water at the level of Hartree-Fock theory plus empirical dispersion. These simulations demonstrate that the "cavity model" of the aqueous electron, in which the spin density of the anionic defect is localized within an excluded volume in the liquid, is stable at room temperature on a time scale of at least several picoseconds. These results validate cavity-forming pseudopotential models of e^-(aq) that have previously been derived from static-exchange Hartree-Fock calculations, and cast doubt upon whether non-cavity-forming pseudopotentials are faithful to the underlying Hartree-Fock calculation from which they were obtained.

Published under license by AIP Publishing. https://doi.org/10.1063/1.5089673

I. INTRODUCTION

The importance of long-range electrostatics in classical molecular dynamics (MD) simulations of condensed-phase systems is by now well established.[1–5] The Ewald summation procedure,[6–13] along with its "particle-mesh" variants,[9–16] is a standard technique for summing the long-range charge-charge interactions in MD simulations performed under periodic boundary conditions (PBC). Ewald summation has also been extended to mixed quantum mechanics/molecular mechanics (QM/MM) simulations,[17–23] under the assumption that the MM region is large compared to the QM region. In that case, it makes sense to approximate the interaction of the QM region with its periodic images by means of classical point charges that are derived from the wave function. With an appropriate correction to the Fock matrix, a fully variational self-consistent field (SCF) procedure is obtained for this QM/MM-Ewald method.[17,18,21]

It remains to specify precisely how the atomic charges are derived from the wave function. The first implementations of the QM/MM-Ewald method relied on Mulliken charges,[17–20,24] which is reasonable for semi-empirical QM calculations in minimal basis sets but leads to serious SCF convergence problems in

Published under license by AIP Publishing

larger basis sets.[21] To circumvent this problem, and to facilitate periodic QM/MM calculations in arbitrary basis sets, we reformulated the QM/MM-Ewald method to use charges derived from the electrostatic potential on a grid,[21] i.e., "CHELPG" charges.[25,26] Because these charges are based on a genuine (in principle, observable) molecular property rather than the atomic orbital overlap matrix, CHELPG charges are stable in large basis sets and in basis sets containing diffuse functions.[21] Our group has used CHELPG charges in a variety of contexts where self-consistent electrostatic embedding charges are required,[27–35] but the analytic gradient of the CHELPG-based QM/MM-Ewald procedure has not yet been reported.

The CHELPG charges are defined via a least-squares fitting problem,[21,26,28] which significantly complicates the QM/MM-Ewald analytic gradient as compared to the version based on Mulliken charges.[22] In the end, however, we obtain a QM/MM method that is far more robust. As a proof-of-concept application, we consider short MD simulations of the aqueous (or "hydrated") electron,[36] e^-(aq), where the need for diffuse basis functions renders previous versions of the QM/MM-Ewald procedure unusable.

The hydrated electron is one of the primary radicals generated by radiolysis of water,[36–41] and despite its definitive experimental identification more than 50 years ago,[42–45] its detailed structure has been a recurring subject of debate.[36,46–50] Prior to 2010, a consensus had seemingly emerged around a "cavity" or "excluded-volume" model,[36] resulting from an electron–water interaction potential that is net repulsive when averaged over all space.[51,52] More recently, however, Schwartz and co-workers have developed an electron–water interaction potential that does *not* behave in this way,[53] and predicts instead a delocalized e^-(aq) wave function. This has led Schwartz *et al.* to question the conventional "cavity model" in a series of papers[53–58] that remain controversial.[52,59–61]

While limited in scope, the simulations presented herein provide strong support for the cavity model. Using only a Hartree-Fock (HF) description of the QM region—the same level of theory used by Schwartz *et al.* to parameterize their electron–water pseudopotential model[53]—our simulations support an excluded volume that is stable in liquid water for >5 ps at T = 300 K. As compared to previous density functional theory (DFT) simulations of this species,[62–66] Hartree-Fock calculations are free from questions regarding self-interaction artifacts that afflict calculations of weakly bound anions,[67,68] as well as those of open-shell solutes in aqueous solution.[69,70] As such, our results provide an important new perspective on the structure of e^-(aq).

II. BACKGROUND REVIEW

In this section, we review the standard Ewald sum and its analytic gradient,[9,10,13] as well as the basic idea behind the QM/MM-Ewald method.[17–19,21,22] This will set the stage for deriving the analytic gradient of the CHELPG-based QM/MM-Ewald method in Secs. III and IV. Detailed derivations of the equations summarized here can be found in the extensive set of Appendixes included in Ref. 22.

Throughout this work, the vector-valued operator $\hat{\nabla}_i$ generates the derivative with respect to the Cartesian coordinates of the ith nucleus, $\mathbf{r}_i = (x_i, y_i, z_i)$,

$$\hat{\nabla}_i f(\mathbf{r}) = \mathbf{u}_x\left(\frac{\partial f}{\partial x_i}\right) + \mathbf{u}_y\left(\frac{\partial f}{\partial y_i}\right) + \mathbf{u}_z\left(\frac{\partial f}{\partial z_i}\right). \tag{2.1}$$

The quantities $\mathbf{u}_x$, $\mathbf{u}_y$, and $\mathbf{u}_z$ are the unit vectors in the indicated directions. For functions $f(r_{ij})$ of the inter-particle distances

$$r_{ij} = \|\mathbf{r}_{ij}\| = \|\mathbf{r}_i - \mathbf{r}_j\|, \tag{2.2}$$

the vector-valued gradient is

$$\hat{\nabla}_i f(r_{ij}) = \left(\frac{\partial f}{\partial r_{ij}}\right)\frac{\mathbf{r}_{ij}}{r_{ij}} = -\hat{\nabla}_j f(r_{ij}). \tag{2.3}$$

A. Ewald sum and its gradient

We wish to solve the usual Ewald problem,[10–12] namely, evaluation of the infinite sum

$$E_{\text{elst}} = \frac{1}{2}\sum_{\mathbf{n}}\sum_{i,j}{}' \frac{q_i q_j}{\|\mathbf{r}_{ij} + \mathbf{n}\|}, \tag{2.4}$$

in which the sums over i and j represent all particles in the unit cell ($\mathbf{n} = \mathbf{0}$) and the primed summation means that $i = j$ is excluded when $\mathbf{n} = \mathbf{0}$, to avoid self-interaction. The quantity

$$\mathbf{n} = n_x L_x \mathbf{u}_x + n_y L_y \mathbf{u}_y + n_z L_z \mathbf{u}_z \tag{2.5}$$

is a lattice vector of the orthorhombic $L_x \times L_y \times L_z$ unit cell, with $(n_x, n_y, n_z) \in \mathbb{Z}^3$. We use atomic units throughout this work, to avoid factors of $(4\pi\varepsilon_0)^{-1}$ in Eq. (2.4) and elsewhere. Our notation largely follows that in Ref. 12 and is slightly modified with respect to our own previous work.[21,22]

According to the usual Ewald procedure, the total electrostatic energy is partitioned into five terms,[11,21,22,71]

$$E_{\text{elst}} = E_{\text{real}} + E_{\text{recip}} + E_{\text{self}} + E_{\text{charge}} + E_{\text{dipole}}. \tag{2.6}$$

The real- and reciprocal-space energies (E_{real} and E_{recip}, respectively) partition the sum in Eq. (2.4) into short- and long-range contributions, with a self-energy correction E_{self} whose origin is discussed below. The final two terms are corrections in cases where the simulation cell has a non-zero net charge or net dipole moment. The rest of this section introduces these terms one by one, along with the analytic gradient of each.

The real-space energy E_{real} is computed using an attenuated Coulomb interaction $\text{erfc}(\eta r)/r$ that decays to zero on a length scale $\sim\eta^{-1}$, where η is the usual Ewald "splitting" parameter. This term is given by[10–12,22,71]

$$E_{\text{real}} = \frac{1}{2}\sum_{\mathbf{n}}\sum_{i,j}{}' q_i q_j \left(\frac{\text{erfc}\left(\eta\|\mathbf{r}_{ij} + \mathbf{n}\|\right)}{\|\mathbf{r}_{ij} + \mathbf{n}\|}\right). \tag{2.7}$$

As in Eq. (2.4), the primed summation excludes $i = j$ when $\mathbf{n} = \mathbf{0}$. If η is chosen such that $\eta^{-1} \ll L/2$ (the "minimum-image convention"[72]), then terms with $\mathbf{n} \neq \mathbf{0}$ make negligible contributions to E_{real} and the sum over $\mathbf{n}$ can be omitted from Eq. (2.7). We leave this sum in place for generality, as the selection of η for QM/MM calculations may be subject to different considerations as compared to purely

Published under license by AIP Publishing

classical Ewald summation.[21] The gradient of E_{real} is straightforward to obtain,[11,22]

$$\hat{\nabla}_i E_{\text{real}} = \sum_{\mathbf{n}} \sum_{j \neq i} q_i q_j \left[\frac{\operatorname{erfc}\left(\eta \|\mathbf{r}_{ij} + \mathbf{n}\|\right)}{\|\mathbf{r}_{ij} + \mathbf{n}\|} + \left(\frac{2\eta}{\sqrt{\pi}}\right) e^{-\eta^2 \|\mathbf{r}_{ij} + \mathbf{n}\|^2} \right] \frac{\mathbf{r}_{ij} + \mathbf{n}}{\|\mathbf{r}_{ij} + \mathbf{n}\|^2}. \tag{2.8}$$

The restriction $j \neq i$ arises from the fact that the $i = j$ case is already excluded for $\mathbf{n} = \mathbf{0}$ in Eq. (2.4), lest we count an atom's Coulomb interaction with itself, whereas for $\mathbf{n} \neq \mathbf{0}$ and $i = j$, the distance $\mathbf{r}_{ij} + \mathbf{n}$ is equal to $\mathbf{n}$, which does not depend on $\mathbf{r}_i$.

We next wish to consider the reciprocal-space energy E_{recip} and its gradient. These will be expressed in terms of the crystallographic structure factor[9,12]

$$S(\mathbf{k}) = \sum_i q_i e^{\imath \mathbf{k} \cdot \mathbf{r}_i}. \tag{2.9}$$

The quantity $\mathbf{k}$ is a reciprocal lattice vector with components $k_\alpha = 2\pi m_\alpha / L_\alpha$, for $\alpha \in \{x, y, z\}$, and $m_\alpha \in \mathbb{Z}$. The quantity $S(\mathbf{k})$ is sometimes denoted $\tilde{\rho}(\mathbf{k})$, as it is a Fourier component of the periodically-replicated charge density $\rho(\mathbf{r})$ arising from the point charges $\{q_i\}$.[11,13,73] Note that

$$|S(\mathbf{k})|^2 = \sum_{i,j} q_i q_j e^{\imath \mathbf{k} \cdot \mathbf{r}_{ij}}. \tag{2.10}$$

As discussed below, we will eventually need to make a distinction between QM charges (derived from the wave function) and MM charges (obtained from a force field),[21] because this distinction affects how Eq. (2.10) is handled. Assuming that the indices i and j are equivalent, which is indeed the case for strictly classical Ewald summation, then Eq. (2.10) can be rewritten as

$$|S(\mathbf{k})|^2 = \Gamma_{\text{s}}(\mathbf{k})^2 + \Gamma_{\text{c}}(\mathbf{k})^2, \tag{2.11}$$

where

$$\Gamma_{\text{s}}(\mathbf{k}) = \sum_j q_j \sin(\mathbf{k} \cdot \mathbf{r}_j), \tag{2.12a}$$

$$\Gamma_{\text{c}}(\mathbf{k}) = \sum_j q_j \cos(\mathbf{k} \cdot \mathbf{r}_j). \tag{2.12b}$$

The reciprocal-space energy can now be written in a compact form,[10–12,17,22]

$$E_{\text{recip}} = \frac{1}{2} \sum_{\mathbf{k} \neq \mathbf{0}} \omega(k) |S(\mathbf{k})|^2, \tag{2.13}$$

where $k = \|\mathbf{k}\|$ and

$$\omega(k) = \left(\frac{4\pi}{Vk^2}\right) e^{-k^2/4\eta^2}. \tag{2.14}$$

The quantity V is the volume of the unit cell. Note that $\omega(k)$ is independent of the coordinates of the particles $\{q_i\}$, so the gradient of E_{recip} is simply[11,22]

$$\hat{\nabla}_i E_{\text{recip}} = \frac{1}{2} \sum_{\mathbf{k} \neq \mathbf{0}} \omega(k) \, \hat{\nabla}_i |S(\mathbf{k})|^2. \tag{2.15}$$

The requisite gradient of $|S(\mathbf{k})|^2$ is

$$\hat{\nabla}_i |S(\mathbf{k})|^2 = -2 q_i \mathbf{k} \sum_j q_j \sin(\mathbf{k} \cdot \mathbf{r}_{ij}). \tag{2.16}$$

Note that the summand in this equation vanishes when $i = j$.

The expression in Eq. (2.16) can be used regardless of whether q_i and q_j are QM or MM point charges. If both i and j represent MM atoms, however, then both summations in Eq. (2.10) run over the same set of atoms, which provides opportunity for some simplification. In this case, a more computationally efficient form of Eq. (2.16) is

$$\hat{\nabla}_i |S(\mathbf{k})|^2 = 2 q_i \mathbf{k} \left[\Gamma_{\text{s}}(\mathbf{k}) \cos(\mathbf{k} \cdot \mathbf{r}_i) - \Gamma_{\text{c}}(\mathbf{k}) \sin(\mathbf{k} \cdot \mathbf{r}_i) \right], \tag{2.17}$$

which makes use of the same equivalence between summation indices i and j that was used to derive Eq. (2.11) from Eq. (2.10). In strictly classical simulations, Eq. (2.17) is used rather than Eq. (2.16) because the sums in Eq. (2.12) can be computed once per time step and reused. This eliminates a double summation over atomic indices that would otherwise be required to evaluate the reciprocal-space gradient in Eq. (2.15). For QM/MM simulations, however, one must consider cases where q_i in Eq. (2.10) is an MM charge but q_j is the charge on a QM atom, and in such cases, Eq. (2.16) must be used rather than Eq. (2.17).

The remaining contributions to the electrostatic energy in Eq. (2.6) are the self energy (E_{self}), charge correction (E_{charge}), and surface-dipole correction (E_{dipole}). We will describe each in turn, starting with

$$E_{\text{self}} = -\frac{\eta}{\sqrt{\pi}} \sum_i q_i^2. \tag{2.18}$$

In a careful derivation of Ewald summation using a Gaussian screening potential for each of the charges q_i, this term arises from the need to eliminate the interaction between q_i with its compensating Gaussian background charge.[73] Stated differently, by including E_{self} in the total electrostatic energy [Eq. (2.6)], we guarantee that the electrostatic potential at the point $\mathbf{r}_i$ does not contain a contribution from the point charge q_i that is located there.[74]

If all of the charges q_i are fixed, then E_{self} has zero gradient with respect to displacements of the nuclei and does not contribute to the dynamics, though it obviously needs to be included if for some reason the charges are modified during a simulation, e.g., in the "charging" (particle insertion) step of a free energy calculation. In the present context, the charges on the QM nuclei are *not* fixed and certainly have non-vanishing gradients with respect to displacements of the nuclear positions. That said, a self-energy term involving the QM charges does not arise in our approach due to the manner in which the QM/MM interactions are handled.[18,22] The summation in Eq. (2.18) thus includes MM charges only, unlike the other equations in this section where the charges $\{q_j\}$ include both QM and MM point charges. This point is discussed further in Sec. II B, where we introduce our QM/MM approach.

The charge correction

$$E_{\text{charge}} = -\frac{\pi Q^2}{2 V \eta^2} \tag{2.19}$$

arises whenever the unit cell contains a non-zero net charge, $Q = \sum_i q_i$.[11,22] This correction amounts to a uniform shift in the potential such that the Ewald potential averages to zero over the unit cell, even when $Q \neq 0$.[75] This corresponds to zeroing out the contribution from the divergent $\mathbf{k} = \mathbf{0}$ Fourier mode that is excluded in E_{recip} [Eq. (2.13)], which is the only meaningful way to

Published under license by AIP Publishing

set the condition of "zero potential at infinite separation" in a periodic system.[76] Equivalently, E_{charge} is the electrostatic interaction energy of a compensating background charge $-Q$, whose uniformity ensures that the charge-correction term engenders no force on the nuclei.[11,77]

Due to its dependence on V^{-1}, what we call E_{charge} has also been interpreted as a correction for the finite volume of the simulation cell.[71,76] Even in QM/MM simulations this correction has a vanishing gradient provided that the total charge Q is fixed. Care must be taken when using Ewald summation in a simulation where either the total charge Q or else the volume of the simulation cell V is modified, but isobaric simulations with fixed total charge should not be problematic.

Finally, there is the dipolar correction E_{dipole} in Eq. (2.6),[8] which is known synonymously as the "surface term"[74,78–80] or sometimes the "polarization term."[5] It arises from the neglected $\mathbf{k} = \mathbf{0}$ term in the reciprocal-space sum [Eq. (2.13)], in cases where the simulation cell has a non-vanishing dipole moment $\mathbf{M} = \sum_i q_i \mathbf{r}_i$. The form of this dipole correction is

$$E_{\text{dipole}} = -\frac{2\pi \|\mathbf{M}\|^2}{(2\varepsilon + 1)V}, \tag{2.20}$$

where ε is the dielectric constant of a medium that is assumed to surround a *supercell* consisting of the unit cell and its periodic images. (See Ref. 80 for a detailed discussion.) The gradient of E_{dipole} is[12,78]

$$\hat{\nabla}_i E_{\text{dipole}} = \frac{4\pi q_i \mathbf{M}}{(2\varepsilon + 1)V}. \tag{2.21}$$

Both E_{dipole} and its gradient vanish under "tin-foil" boundary conditions, corresponding to the limit $\varepsilon \to \infty$. We assume tin-foil boundary conditions in this work and thus neglect E_{dipole}.

B. QM/MM-Ewald method

The partition between real space and reciprocal space is slightly different in the QM/MM-Ewald method as compared to that used in the classical Ewald summation technique. In the traditional approach, η is chosen to balance efficient convergence of the real- and reciprocal-space sums,[9] often resulting in values $\eta^{-1} \approx L/2$. Coulomb interactions are then summed in real space within the range of the attenuated Coulomb potential $\text{erfc}(\eta r)/r$. In contrast, the procedure used here involves a real-space sum of all QM-MM interactions *within the unit cell*, using the QM density to compute the electrostatic interaction with the MM point charges. To this we then add a correction ΔE^{PBC} that accounts for interactions between the QM region and the periodic images of that cell.[21] It is the latter correction (only) that uses a point-charge approximation to the QM electron density.

With this in mind, we write the total energy of the periodically replicated QM/MM system as[17,21]

$$E = E^{\text{RS}}_{\text{QM}} + E^{\text{RS}}_{\text{QM-MM}} + E^{\text{PBC}}_{\text{MM}} + \Delta E^{\text{PBC}}. \tag{2.22}$$

The superscript "RS" means "real space" and refers to the unit cell itself. The quantity $E^{\text{RS}}_{\text{QM}}$ is simply the electronic structure energy, and $E^{\text{RS}}_{\text{QM-MM}}$ is obtained by direct evaluation of the interaction between the QM density and the MM point charges that are contained within the unit cell. The quantity $E^{\text{PBC}}_{\text{MM}}$ is simply the mutual electrostatic energy of all the MM point charges under PBC, including both the unit cell and the image cells. It is computed using conventional Ewald summation and need not be discussed further.

It remains to account for the interaction of the QM region in the unit cell with the periodic replicas of both the QM and the MM regions, and this comprises the final term in Eq. (2.22). We separate this correction into two parts,

$$\Delta E^{\text{PBC}} = \Delta E^{\text{PBC}}_{\text{QM-QM}} + \Delta E^{\text{PBC}}_{\text{QM-MM}}. \tag{2.23}$$

The first term, $\Delta E^{\text{PBC}}_{\text{QM-QM}}$, represents the interaction of the QM region with its own periodic images, whereas the second term represents the interaction between the QM region in the unit cell and the MM charges in the replica cells. In either case, we replace the QM region and its periodic images with a set of atom-centered point charges for the purpose of computing these interactions; see Fig. 1.

Whereas in Sec. II A, we presented the Ewald formalism in terms of a generic set of charges, here we need to be precise about the distinction between charges $\{q_i\}$ that are located on MM atoms and assumed to be fixed, vs charges that are located on QM atoms. The latter, which we will denote by $\{Q_A\}$, are derived from the QM wave function in some way and thus have non-vanishing derivatives as the nuclei are displaced.

Implicit in our approach is an assumption that the QM region is small compared to the MM region, the latter of which has size L.

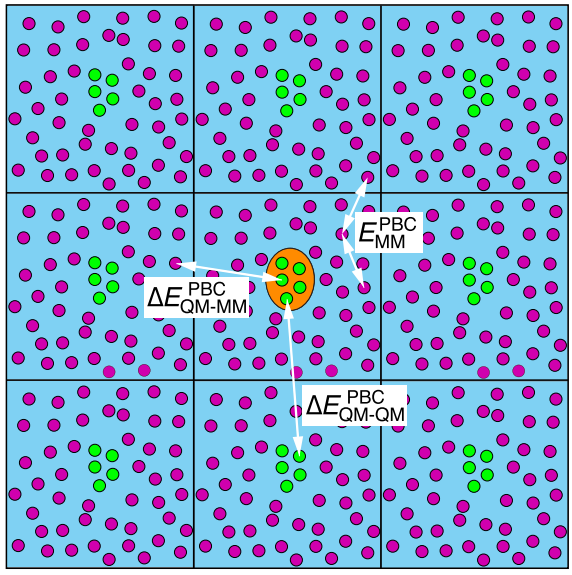

FIG. 1. Cartoon diagram illustrating how the electrostatic interactions are partitioned in the QM/MM-Ewald method. The central (unit) cell contains a QM density, depicted as an orange ellipse, from which a set of green charges $\{Q_A\}$ are derived. The MM point charges $\{q_i\}$ are shown in purple. We illustrate examples of the two types of interactions that define $\Delta E^{\text{PBC}} = \Delta E^{\text{PBC}}_{\text{QM-QM}} + \Delta E^{\text{PBC}}_{\text{QM-MM}}$, as well as those that define $E^{\text{PBC}}_{\text{MM}}$.

Published under license by AIP Publishing

It then makes sense to define[17,21]

$$\Delta E^{\mathrm{PBC}}_{\mathrm{QM\text{-}QM}} = \frac{1}{2}\sum_{A,B}^{N_{\mathrm{QM}}} Q_A\, Q_B\, \varphi(\mathbf{r}_{AB}), \tag{2.24a}$$

$$\Delta E^{\mathrm{PBC}}_{\mathrm{QM\text{-}MM}} = \sum_{A}^{N_{\mathrm{QM}}}\sum_{i}^{N_{\mathrm{MM}}} Q_A\, q_i\, \varphi(\mathbf{r}_{Ai}), \tag{2.24b}$$

where $\varphi(\mathbf{r})$ is the effective pair potential arising from Ewald summation, with $\mathbf{r}_{AB} = \mathbf{r}_A - \mathbf{r}_B$ and $\mathbf{r}_{Ai} = \mathbf{r}_A - \mathbf{r}_i$. This potential is given by[8,12,17,22,71,72]

$$\varphi(\mathbf{r}) = \sum_{\mathbf{k}\neq\mathbf{0}} \omega(k)\cos(\mathbf{k}\cdot\mathbf{r}) - \frac{\mathrm{erf}(\eta r)}{r} + \sum_{\mathbf{n}\neq\mathbf{0}} \frac{\mathrm{erfc}\big(\eta\|\mathbf{r}+\mathbf{n}\|\big)}{\|\mathbf{r}+\mathbf{n}\|}. \tag{2.25}$$

(A detailed derivation can be found in Appendix D of Ref. 22.) The quantities $\varphi(\mathbf{r}_{AB})$ and $\varphi(\mathbf{r}_{Ai})$ that are needed in Eq. (2.24) each depend on the coordinates of the atoms, but both are *independent* of the details of the electronic structure. As such, the potential $\varphi(\mathbf{r})$ needs to be evaluated, at all of the relevant points $\mathbf{r}_{AB}$ and $\mathbf{r}_{Ai}$, only once per time step in a QM/MM simulation. This is done outside of the SCF iterations.[20,21]

It should also be noted that nothing analogous to the self-energy term E_{self} [Eq. (2.18)] is evident in Eq. (2.24). For interactions between QM and MM charges, the two sums in Eq. (2.24b) run over different sets of charges, so this issue simply does not arise; however, there is no restriction on the summation that defines $\Delta E^{\mathrm{PBC}}_{\mathrm{QM\text{-}QM}}$ in Eq. (2.24a). For $A = B$ in that equation, the Coulomb interaction is given by

$$\lim_{r\to 0}\frac{\mathrm{erf}(\eta r)}{r} = \frac{2\eta}{\sqrt{\pi}}. \tag{2.26}$$

This is, in fact, the self-energy term, but it is included automatically by the potential $\varphi(\mathbf{r})$.

The PBC correction to the energy gives rise to a corresponding correction $\Delta\mathbf{F}^{\mathrm{PBC}}$ to the Fock matrix,

$$\Delta F^{\mathrm{PBC}}_{\mu\nu} = \frac{\partial(\Delta E^{\mathrm{PBC}})}{\partial P_{\mu\nu}} = \sum_{A}^{N_{\mathrm{QM}}} \underbrace{\left(\frac{\partial(\Delta E^{\mathrm{PBC}})}{\partial Q_A}\right)}_{\Theta_A}\left(\frac{\partial Q_A}{\partial P_{\mu\nu}}\right). \tag{2.27}$$

For brevity, let us introduce a simplified notation

$$\begin{aligned}\varphi_{AB} &= \varphi(\mathbf{r}_{AB}),\\ \varphi_{Ai} &= \varphi(\mathbf{r}_{Ai}),\end{aligned} \tag{2.28}$$

and note that $\varphi_{BA} = \varphi_{AB}$ since $\varphi(\mathbf{r}) = \varphi(-\mathbf{r})$. We can then write[21]

$$\Theta_A = \frac{\partial(\Delta E^{\mathrm{PBC}})}{\partial Q_A} = \sum_{B}^{N_{\mathrm{QM}}} Q_B\,\varphi_{AB} + \sum_{i}^{N_{\mathrm{MM}}} q_i\,\varphi_{Ai}. \tag{2.29}$$

In this expression, only the charges Q_B change from one SCF iteration to the next. The potentials φ_{AB} and φ_{Ai} are fixed so long as the nuclei do not move.

To complete the correction $\Delta\mathbf{F}^{\mathrm{PBC}}$ in Eq. (2.27), one must specify how the QM charges are obtained from the wave function and then evaluate the derivatives $\partial Q_A/\partial P_{\mu\nu}$. This is discussed in Sec. IV.

III. QM/MM-EWALD GRADIENT

In this section, we develop the analytic gradient of the QM/MM-Ewald method that was introduced in Ref. 21 and summarized above. Detailed derivations of the results presented in this section can be found in an extensive set of Appendixes in Ref. 22.

A. Ewald gradient

The gradient of ΔE^{PBC} with respect to a nuclear displacement is different depending upon whether it is a QM or an MM nucleus that is displaced. We first consider the derivative $\partial\Delta E^{\mathrm{PBC}}/\partial x_i$ with respect to a Cartesian coordinate x_i for the MM charge q_i. Note that $\partial q_j/\partial x_i = 0$ for $i \neq j$, because the MM charges have fixed values, but that $\partial Q_A/\partial x_i$ does *not* vanish, because the wave function is perturbed by displacement of q_i. A straightforward calculation based on Eqs. (2.23) and (2.24) affords

$$\frac{\partial\Delta E^{\mathrm{PBC}}}{\partial x_i} = \sum_{A}^{N_{\mathrm{QM}}}\left[q_i\, Q_A\left(\frac{\partial\varphi_{Ai}}{\partial x_i}\right) + \Theta_A\left(\frac{\partial Q_A}{\partial x_i}\right)\right], \tag{3.1}$$

where Θ_A was defined in Eq. (2.29).

We next consider displacement of a QM nucleus along Cartesian coordinate x_A. Given that the $\{q_i\}$ are fixed, one obtains

$$\begin{aligned}\frac{\partial\Delta E^{\mathrm{PBC}}}{\partial x_A} = &\sum_{B}^{N_{\mathrm{QM}}} Q_A\, Q_B\left(\frac{\partial\varphi_{AB}}{\partial x_B}\right)(1-\delta_{AB}/2) + \sum_{i}^{N_{\mathrm{MM}}} Q_A\, q_i\left(\frac{\partial\varphi_{Ai}}{\partial x_A}\right)\\ &+ \sum_{B,C}^{N_{\mathrm{QM}}}\left(\frac{\partial Q_B}{\partial x_A}\right) Q_C\,\varphi_{BC} + \sum_{i}^{N_{\mathrm{MM}}}\sum_{B}^{N_{\mathrm{QM}}} q_i\left(\frac{\partial Q_B}{\partial x_A}\right)\varphi_{Bi}.\end{aligned} \tag{3.2}$$

With regard to the first term, note that $\delta_{AB} = 0$ unless $A = B$, but the function $\varphi_{AA} \equiv \varphi(\mathbf{0})$ is a constant so $\partial\varphi_{AA}/\partial x_A = 0$. The δ_{AB}-dependent term in Eq. (3.2) therefore vanishes. Use of this fact, along with the definition of Θ_A in Eq. (2.29), affords

$$\frac{\partial\Delta E^{\mathrm{PBC}}}{\partial x_A} = \sum_{B}^{N_{\mathrm{QM}}} Q_A Q_B\left(\frac{\partial\varphi_{AB}}{\partial x_A}\right) + \sum_{i}^{N_{\mathrm{MM}}} q_i Q_A\left(\frac{\partial\varphi_{Ai}}{\partial x_A}\right) + \sum_{B}^{N_{\mathrm{QM}}}\Theta_B\left(\frac{\partial Q_B}{\partial x_A}\right). \tag{3.3}$$

Expressions for the charge derivatives $\partial Q_B/\partial x_A$ are not universal and depend upon how the QM charges are obtained from the wave function. These derivatives are taken up in Sec. IV.

In contrast, the derivative of the Ewald potential with respect to x_A *is* universal and is given by

$$\begin{aligned}\hat{\nabla}_A\,\varphi_{Ai} = &\left[\frac{\mathrm{erf}(\eta\, r_{Ai})}{r_{Ai}} - \left(\frac{2\eta}{\sqrt{\pi}}\right)e^{-\eta^2 r_{Ai}^2}\right]\frac{\mathbf{r}_{Ai}}{r_{Ai}^2} - \sum_{\mathbf{k}\neq\mathbf{0}}\mathbf{k}\,\omega(k)\sin(\mathbf{k}\cdot\mathbf{r}_{Ai})\\ &- \sum_{\mathbf{n}\neq\mathbf{0}}\left[\frac{\mathrm{erfc}\big(\eta\|\mathbf{r}_{Ai}+\mathbf{n}\|\big)}{\|\mathbf{r}_i+\mathbf{n}\|} + \left(\frac{2\eta}{\sqrt{\pi}}\right)e^{-\eta^2\|\mathbf{r}_{Ai}+\mathbf{n}\|^2}\right]\frac{\mathbf{r}_{Ai}+\mathbf{n}}{\|\mathbf{r}_{Ai}+\mathbf{n}\|^2}.\end{aligned} \tag{3.4}$$

The function $\omega(k)$ is defined in Eq. (2.14), and for generality we have opted for the use of Eq. (2.16), rather than Eq. (2.17). (Regarding this point, see the discussion in Sec. II.) The gradient $\hat{\nabla}_A\,\varphi_{AB}$ can be obtained from Eq. (3.4) simply by replacing i with B as there is nothing in the form of $\varphi(\mathbf{r})$ that depends on the identity of the charges.

Published under license by AIP Publishing

The derivative of $\varphi(\mathbf{r})$ with respect to displacement of an MM charge is easily obtained from Eq. (3.4) by recognizing that

$$\hat{\nabla}_A \varphi_{Ai} = -\hat{\nabla}_i \varphi_{Ai}. \tag{3.5}$$

B. SCF energy gradient

The derivative of the Hartree-Fock energy $\mathcal{E}_{\mathrm{HF}}$ with respect to a perturbation x is denoted $\mathcal{E}^x_{\mathrm{HF}} \equiv \partial\mathcal{E}_{\mathrm{HF}}/\partial x$, and we use similar notation for other derivatives such as $H^x_{\mu\nu} \equiv \partial H_{\mu\nu}/\partial x$, where $H_{\mu\nu}$ represents the one-electron (or "core") Hamiltonian. The Hartree-Fock energy gradient can be expressed as[81]

$$\mathcal{E}^x_{\mathrm{HF}} = \mathcal{E}^{[x]}_{\mathrm{HF}} + \sum_{\mu\nu} P^x_{\mu\nu} F_{\mu\nu}, \tag{3.6}$$

where

$$F_{\mu\nu} = H_{\mu\nu} + \sum_{\lambda\sigma} (\mu\nu||\lambda\sigma) P_{\lambda\sigma} \tag{3.7}$$

is the Fock matrix and

$$\mathcal{E}^{[x]}_{\mathrm{HF}} = \sum_{\mu\nu} P_{\mu\nu} H^x_{\mu\nu} + \frac{1}{2} \sum_{\mu\nu\lambda\sigma} P_{\mu\nu} (\mu\nu||\lambda\sigma)^x P_{\lambda\sigma} + V^x_{\mathrm{nuc}} \tag{3.8}$$

is the Hellmann-Feynman part of the energy gradient, which has the same form as the Hartree-Fock energy but with differentiated integrals. (What we call the "Hellmann-Feynman" contribution has also been called a "skeleton" derivative.[82]) These equations are adaptable to DFT in a straightforward way, so for brevity we do not include the exchange-correlation term in the derivation that follows. DFT is included in our implementation, however.

It was shown long ago that Eq. (3.6) is needlessly expensive[81] because the density matrix derivatives $P^x_{\mu\nu} \equiv \partial P_{\mu\nu}/\partial x$ can be eliminated in favor of the energy-weighted density matrix

$$W_{\mu\nu} = \sum_i^{\mathrm{occ}} \epsilon_i c^*_{\mu i} c_{\nu i}. \tag{3.9}$$

The occupied orbital eigenvalues ϵ_i and coefficients $c_{\mu i}$ are solutions of the SCF equation

$$\mathbf{Fc} = \epsilon\mathbf{Sc}, \tag{3.10}$$

where $\mathbf{S}$ is the atomic orbital overlap matrix. The Hartree-Fock energy gradient is then

$$\mathcal{E}^x_{\mathrm{HF}} = \mathcal{E}^{[x]}_{\mathrm{HF}} - \sum_{\mu\nu} W_{\mu\nu} S^x_{\mu\nu}. \tag{3.11}$$

Derivation of Eq. (3.11) from Eq. (3.6) relies on the condition $\mathbf{c}^\dagger\mathbf{Sc} = \mathbf{1}$, in addition to Eq. (3.10).[81]

C. Total gradient

Now let us consider the energy

$$\mathcal{E} = \mathcal{E}_{\mathrm{HF}} + \Delta E^{\mathrm{PBC}} \tag{3.12}$$

under PBC. The gradient $\partial\mathcal{E}/\partial x$ contains additional terms with respect to the usual Hartree-Fock gradient, whose form can be seen in Eq. (3.2). The result can be regrouped into a Hellmann-Feynman part $\mathcal{E}^{[x]}$ and a "response" part, à la Eq. (3.6). For a perturbation along QM nuclear coordinate x_A, the total energy gradient is

$$\frac{\partial\mathcal{E}}{\partial x_A} = \mathcal{E}^{[x_A]} + \sum_{\mu\nu}\left(\frac{\partial P_{\mu\nu}}{\partial x_A}\right) F_{\mu\nu} + \sum_B^{N_{\mathrm{QM}}} \underbrace{\left(\frac{\partial(\Delta E^{\mathrm{PBC}})}{\partial Q_B}\right)}_{\Theta_B} \left(\frac{\partial Q_B}{\partial x_A}\right). \tag{3.13}$$

The Hellmann-Feynman part is

$$\mathcal{E}^{[x_A]} = \mathcal{E}^{[x_A]}_{\mathrm{HF}} + \sum_i^{N_{\mathrm{MM}}} q_i Q_A \left(\frac{\partial\varphi_{Ai}}{\partial x_A}\right) + \sum_B^{N_{\mathrm{QM}}} Q_A Q_B \left(\frac{\partial\varphi_{AB}}{\partial x_A}\right). \tag{3.14}$$

We next use the chain rule to rewrite the charge derivative $\partial Q_B/\partial x_A$ in Eq. (3.13) in the form

$$\frac{\partial Q_B}{\partial x_A} = \sum_{\mu\nu}\left(\frac{\partial Q_B}{\partial P_{\mu\nu}}\right)\left(\frac{\partial P_{\mu\nu}}{\partial x_A}\right) + \sum_M \left(\frac{\partial Q_B}{\partial M}\right)\left(\frac{\partial M}{\partial x_A}\right). \tag{3.15}$$

The quantity M represents anything on which the QM charge Q_B depends *except* for the density matrix, since dependence on $P_{\mu\nu}$ is included explicitly in Eq. (3.15). When Mulliken charges are used, for example, then Q_B depends on the overlap matrix so $M \equiv S_{\mu\nu}$ in that case. These "M-derivatives," which encode an implicit, charge-response contribution to the gradient, will be evaluated in Sec. IV, for both Mulliken and CHELPG charges.

By separating out the density matrix dependence, the $P_{\mu\nu}$-dependent part of the final term in Eq. (3.13) can be written as

$$\sum_B^{N_{\mathrm{QM}}} \sum_{\mu\nu} \Theta_B \left(\frac{\partial Q_B}{\partial P_{\mu\nu}}\right)\left(\frac{\partial P_{\mu\nu}}{\partial x_A}\right) = \sum_{\mu\nu}\left(\frac{\partial P_{\mu\nu}}{\partial x_A}\right)\Delta F^{\mathrm{PBC}}_{\mu\nu} \tag{3.16}$$

using Eq. (2.27). The total gradient in Eq. (3.13) then becomes

$$\frac{\partial\mathcal{E}}{\partial x_A} = \mathcal{E}^{[x_A]} + \Theta^{[x_A]} + \sum_{\mu\nu}\left(\frac{\partial P_{\mu\nu}}{\partial x_A}\right)(F_{\mu\nu} + \Delta F^{\mathrm{PBC}}_{\mu\nu}), \tag{3.17}$$

where

$$\Theta^{[x_A]} = \sum_B^{N_{\mathrm{QM}}} \Theta_B \sum_M \left(\frac{\partial Q_B}{\partial M}\right)\left(\frac{\partial M}{\partial x_A}\right) \tag{3.18}$$

is a charge-response term evaluated for a fixed density matrix. The crucial observation from Eq. (3.17) is that the derivation of the response terms in the normal SCF gradient, i.e., the $-\mathbf{WS}^x$ term in Eq. (3.11), can be carried over to describe the term containing $F_{\mu\nu} + \Delta F^{\mathrm{PBC}}_{\mu\nu}$ in Eq. (3.17). The Fock matrix is modified, to reflect the modified energy $\mathcal{E}_{\mathrm{HF}} + \Delta E^{\mathrm{PBC}}$ that includes the PBC correction, but otherwise all of the formalism of the SCF gradient carries over, without the need to evaluate explicit density matrix derivatives $\partial P_{\mu\nu}/\partial x_A$. As such, the cost to evaluate the QM/MM-Ewald gradient remains comparable to the cost of the normal SCF energy gradient. In particular, solution of coupled-perturbed SCF equations[81] (to obtain $\partial P_{\mu\nu}/\partial x_A$) is not required.

For definiteness, we go one step further in explicating the final gradient expression,

$$\frac{\partial\mathcal{E}}{\partial x_A} = \mathcal{E}^{x_A}_{\mathrm{HF}} + \Theta^{[x_A]} + \sum_B^{N_{\mathrm{QM}}} Q_A Q_B \left(\frac{\partial\varphi_{AB}}{\partial x_A}\right) + \sum_i^{N_{\mathrm{MM}}} q_i Q_A \left(\frac{\partial\varphi_{Ai}}{\partial x_A}\right). \tag{3.19}$$

The quantity $\mathcal{E}^{x_A}_{\mathrm{HF}}$ is the traditional Hartree-Fock energy gradient [Eq. (3.11)], evaluated using the PBC-corrected Fock matrix $\mathbf{F} + \Delta\mathbf{F}^{\mathrm{PBC}}$. Of the three additional terms in Eq. (3.19) that arise from the PBC, two of them simply involve derivatives of $\varphi(\mathbf{r})$ and can be

Published under license by AIP Publishing

evaluated using Eq. (3.4). The charge-response term $\Theta^{[x_A]}$ involves derivatives of the QM atomic charges that are discussed in Sec. IV, once we have defined how the QM charges Q_B are to be obtained from the wave function. Without that information, this is as far as we can take the derivation of the analytic gradient.

In comparison with Eq. (3.19), the energy derivative for displacement of an MM charge is much simpler. For the displacement of q_i along Cartesian coordinate x_i, the analogue of Eq. (3.15) is simply

$$\frac{\partial Q_B}{\partial x_i} = \sum_{\mu\nu}\left(\frac{\partial Q_B}{\partial P_{\mu\nu}}\right)\left(\frac{\partial P_{\mu\nu}}{\partial x_i}\right). \tag{3.20}$$

The "M-derivative" term in Eq. (3.15) is absent here because quantities such as $S_{\mu\nu}$ that are needed to evaluate the QM charges are independent of the positions of the MM atoms. (The same is true of other quantities needed to evaluate CHELPG charges, such as electrostatic potential grid points that may be tied to the location of the QM atoms but are independent of the positions of the MM charges.) This also means that there is no $\mathbf{WS}^x$ term in the derivative $\partial\mathcal{E}_{\mathrm{HF}}/\partial x_i$. Perturbation of x_i only affects the core Hamiltonian and the internuclear potential. The analytic gradient is

$$\frac{\partial\mathcal{E}}{\partial x_i} = \sum_{\mu\nu} P_{\mu\nu}\left(\frac{\partial H_{\mu\nu}}{\partial x_i}\right) + \frac{\partial V_{\mathrm{nuc}}}{\partial x_i} + \sum_{B}^{N_{\mathrm{QM}}} q_i\, Q_B\left(\frac{\partial\varphi_{Bi}}{\partial x_i}\right). \tag{3.21}$$

Again, no explicit derivatives of $P_{\mu\nu}$ are required.

IV. CHARGE DERIVATIVES

The final missing contribution to the QM/MM-Ewald gradient is the "M-derivative" (charge response with fixed density matrix) term that is defined in Eqs. (3.15) and (3.18). The quantity M in these equations represents any independent variable upon which Q_A depends *except* for $P_{\mu\nu}$. The exception arises because dependence on $P_{\mu\nu}$ is already folded into the energy-weighted density matrix, i.e., the $-\mathbf{WS}^x$ term of the traditional Hartree-Fock gradient.

To proceed further, we must decide how Q_A will be determined from the QM calculation. The original minimal-basis formulation of the QM/MM-Ewald method used Mulliken charges,[17–20,24] but these perform poorly in larger basis sets, sometimes leading to SCF convergence failure.[21] Even in modest (albeit non-minimal) basis sets, we sometimes encounter problems with the Mulliken-based procedure when the QM region is large. In the interest of completeness, however, we will nonetheless present the formalism for Mulliken charges in Sec. IV A, followed by the much more complicated formalism for CHELPG charges in Sec. IV B.

A. Mulliken charges

The Mulliken charge for atom A is

$$Q_A = Z_A - \sum_{\mu\in A}\sum_{\nu} P_{\mu\nu}S_{\mu\nu}. \tag{4.1}$$

The derivative $\partial Q_A/\partial P_{\mu\nu}$ that is required to construct $\Delta\mathbf{F}^{\mathrm{PBC}}$ [Eq. (2.27)] has been reported in previous work.[21,27] In symmetrized form, it is

$$\frac{\partial Q_A}{\partial P_{\mu\nu}} = -\frac{1}{2}\left(S_{\mu\nu}\delta_{\mu\in A} + S_{\nu\mu}\delta_{\nu\in A}\right), \tag{4.2}$$

where $\delta_{\mu\in A} = 1$ if basis function μ is centered on nucleus A and is zero if not.

The independent variables in Eq. (4.1) are $P_{\mu\nu}$ and $S_{\mu\nu}$, so for the purpose of computing the "M-derivatives" in Eq. (3.15), the sum over M runs over all overlap matrix elements $S_{\mu\nu}$. The second term in Eq. (3.15) therefore becomes

$$\begin{aligned}\sum_{M}\left(\frac{\partial Q_B}{\partial M}\right)\left(\frac{\partial M}{\partial x_A}\right) &= \sum_{\mu\nu}\left(\frac{\partial Q_B}{\partial S_{\mu\nu}}\right)\left(\frac{\partial S_{\mu\nu}}{\partial x_A}\right)\\ &= -\sum_{\mu\in B}\sum_{\nu} P_{\mu\nu}\left(\frac{\partial S_{\mu\nu}}{\partial x_A}\right)\end{aligned} \tag{4.3}$$

so that the charge-response contribution to the gradient [Eq. (3.19)] is

$$\Theta^{[x_A]} = -\sum_{B}^{N_{\mathrm{QM}}}\Theta_B\sum_{\mu\in B}\sum_{\nu} P_{\mu\nu}S^{x_A}_{\mu\nu}. \tag{4.4}$$

Recall that Θ_B is defined in Eq. (2.29). This completes the specification of the gradient $\partial\mathcal{E}/\partial x_A$ in the case of Mulliken image charges. Note that evaluation of Eq. (4.4) does not require any new quantities that are not already needed to evaluate the QM/MM-Ewald Hartree-Fock energy and the normal (non-QM/MM) Hartree-Fock gradient.

B. CHELPG charges

CHELPG charges[25,26] are determined by first evaluating the electrostatic potential $\Phi(\mathbf{r})$ generated by the QM region on a set of grid points $\{\mathbf{r}_\alpha\}$. These points are intentionally excluded from regions of space that lie within the van der Waals radius of any QM nucleus, since the goal is to reproduce the potential at points *exterior* to the molecule. Let us denote the electrostatic potential values used in the fit as $\Phi_\alpha = \Phi(\mathbf{r}_\alpha)$. These values are computed according to

$$\Phi_\alpha = \sum_A \frac{Z_A}{R_{\alpha A}} - \sum_{\mu\nu}(\mathbf{I}_\alpha)_{\mu\nu}P_{\mu\nu}, \tag{4.5}$$

where

$$R_{\alpha A} = \|\mathbf{R}_{\alpha A}\| = \|\mathbf{r}_\alpha - \mathbf{r}_A\|. \tag{4.6}$$

The electronic contribution to Φ_α is expressed in terms of one-electron integrals

$$(\mathbf{I}_\alpha)_{\mu\nu} = \left\langle\mu\left|\frac{1}{\|\mathbf{r}-\mathbf{r}_\alpha\|}\right|\nu\right\rangle \tag{4.7}$$

that represent the electrostatic potential generated by the function-pair $\mu\nu$ at the point $\mathbf{r}_\alpha$. [Note that $\mathbf{r}$ in Eq. (4.7) is the integration variable, whereas $\mathbf{r}_\alpha$ is a parameter.]

CHELPG charges are computed via least-squares fit of the values $\{\phi_\alpha\}$ to the data points $\{\Phi_\alpha\}$, where $\phi_\alpha = \phi(\mathbf{r}_\alpha)$ and

$$\phi(\mathbf{r}) = \sum_{A}^{N_{\mathrm{QM}}}\frac{Q_A}{\|\mathbf{r}-\mathbf{r}_A\|} \tag{4.8}$$

Published under license by AIP Publishing

is the electrostatic potential generated by the atom-centered charges $\{Q_A\}$. The fit is constrained to reproduce the net molecular charge, which we denote as

$$Q = \sum_{A}^{N_{QM}} Q_A. \tag{4.9}$$

Operationally, the CHELPG procedure amounts to minimization of a Lagrangian[28]

$$\mathcal{L}(\{Q_A\}) = \sum_{\alpha}^{N_{grid}} w_\alpha (\Phi_\alpha - \phi_\alpha)^2 - \lambda\left(Q - \sum_{B}^{N_{QM}} Q_B\right). \tag{4.10}$$

As written, the fit uses weights $\{w_\alpha\}$ assigned to the points $\{\mathbf{r}_\alpha\}$. The weights can be used, for example, to design a scheme whereby the computed charges $\{Q_A\}$ are rigorously continuous functions of the molecular geometry,[28] or else to prune the grid when atom-centered grids are used, lest the fit put too little weight on regions far from the nuclei.[21] Alternatively, the weights can be set to $w_\alpha = 1$ and thereby ignored, as in the original CHELPG algorithm.[25]

It is reported that the CHELPG least-squares problem may be rank-deficient,[26,83,84] and a variety of alternative procedures have been devised to handle such instances.[26] We have not found these to be necessary. Indeed, the primary criticism of the CHELPG procedure—that it uses atomic charges as fitting parameters and may therefore sacrifice "chemically intuitive" charges in the interest of better fitting the electrostatic potential—is immaterial here. We use CHELPG charges precisely because they produce good molecular electrostatic potentials.

An explicit formula can be given for the charges that minimize $\mathcal{L}$ in Eq. (4.10),[28] but we need some notation first. Define a $N_{QM} \times N_{QM}$ matrix $\mathbf{G}$ whose matrix elements are

$$G_{AB} = \sum_{\alpha}^{N_{grid}} \frac{w_\alpha}{R_{\alpha A} R_{\alpha B}}. \tag{4.11}$$

Also define an N_{QM}-dimensional vector $\mathbf{e}$ whose elements are

$$e_A = \sum_{\alpha}^{N_{grid}} \frac{w_\alpha \Phi_\alpha}{R_{\alpha A}}. \tag{4.12}$$

Then the charges $\{Q_A\}$ that minimize $\mathcal{L}$ are given in vector form by

$$\mathbf{Q} = \mathbf{G}^{-1}\left(\mathbf{e} - \frac{\lambda}{2}\mathbf{1}\right), \tag{4.13}$$

where

$$\lambda = 2\left(\frac{-Q + \sum_A (\mathbf{e}\mathbf{G}^{-1})_A}{\sum_{B,C} (\mathbf{G}^{-1})_{BC}}\right) \tag{4.14}$$

is the value taken by the Lagrange multiplier. After some manipulation, Eq. (4.13) can be placed in a form that is more convenient for the task at hand. This form,

$$Q_A = \sum_B (e_B - \lambda/2)(\mathbf{G}^{-1})_{BA}, \tag{4.15}$$

lends itself to more straightforward differentiation. See Appendix G of Ref. 22 for a detailed derivation of these expressions.

The derivatives $\partial Q_A/\partial P_{\mu\nu}$ that appear in $\Delta F^{PBC}_{\mu\nu}$ [Eq. (2.27)] have been discussed in our previous work,[21] but the formulas are repeated here for completeness. Despite the fact that only one-electron integrals are involved, these quantities represent a computational bottleneck and their evaluation must be handled carefully. We first define

$$\xi_{\alpha A} = \sum_{B}^{N_{QM}} \frac{w_\alpha (\mathbf{G}^{-1})_{BA}}{R_{\alpha B}} \tag{4.16}$$

and

$$\gamma_A = \frac{\sum_B (\mathbf{G}^{-1})_{AB}}{\sum_{C,D} (\mathbf{G}^{-1})_{CD}}, \tag{4.17}$$

both of which are trivial to evaluate (given $\mathbf{G}^{-1}$). We also define matrices

$$(\mathbf{\Omega}_B)_{\mu\nu} = \sum_{\alpha}^{N_{grid}} \xi_{\alpha B} (\mathbf{I}_\alpha)_{\mu\nu}, \tag{4.18}$$

which are relatively expensive to evaluate because they contain the electrostatic potential integrals. The most efficient formulation of the charge derivatives in question can then be written as[21,22]

$$\frac{\partial Q_A}{\partial P_{\mu\nu}} = \sum_{B}^{N_{QM}} (\mathbf{\Omega}_B)_{\mu\nu} (\gamma_A - \delta_{AB}). \tag{4.19}$$

When this expression is used in Eq. (2.27), the result is that construction of $\Delta\mathbf{F}^{PBC}$ requires evaluation of electrostatic potential integrals a total of N_{QM} times,[21] assuming that the primitive integral array $(\mathbf{I}_\alpha)_{\mu\nu}$ is too large to store in core memory. Since $N_{QM} \ll N_{grid}$, the formulation presented above is more efficient than other ways of reordering the summations in question.[21] The formal scaling of Eq. (4.18), and thus the formal scaling to construct $\Delta\mathbf{F}^{PBC}$, is $\mathcal{O}(N_{QM} \times N_{grid} \times N_{fp})$, where $N_{fp} \le N^2_{basis}$ is the number of non-negligible basis function pairs.

To obtain the QM/MM-Ewald analytic energy gradient, we also need expressions for the derivatives $Q^x_A \equiv \partial Q_A/\partial x$ with respect to nuclear displacements. Upon differentiating Eq. (4.15), one obtains[22]

$$Q^x_A = \sum_{B,C}\left[e^x_B (\mathbf{G}^{-1})_{BC} + e_B (\mathbf{G}^{-1})^x_{BC} - (\lambda/2)(\mathbf{G}^{-1})^x_{BC}\right](\delta_{AC} - \gamma_A). \tag{4.20}$$

The derivative λ^x of the Lagrange multiplier, which arises in straightforward differentiation of Eq. (4.15), has been rewritten in the form of the γ_A-dependent terms in Eq. (4.20). (See Appendix H of Ref. 22 for a detailed derivation.) Still, Eq. (4.20) is deceptively compact because while $(\mathbf{G}^{-1})^x_{BC}$ and e^x_B can be expressed in analytic form, the expressions are rather involved. These derivatives are presented below.

One complexity is the appearance of the grid points $\mathbf{r}_\alpha$ in the definitions of $\mathbf{e}$ and $\mathbf{G}$. As originally formulated,[25,26] the CHELPG algorithm relies on Cartesian grids, in which case the locations of the $\{\mathbf{r}_\alpha\}$ are independent of any displacements of the QM nuclei. While the computational overhead associated with CHELPG charges is negligible when these charges are computed as an after-the-fact analysis tool, it becomes significant in QM/MM simulations because the charges and their derivatives $\partial Q_A/\partial P_{\mu\nu}$ must be recomputed at

Published under license by AIP Publishing

each SCF cycle. To mitigate this cost, we have previously introduced a modified CHELPG algorithm that uses atom-centered grids.[21] While this significantly reduces the number of grid points required to obtain a good fit, it increases the complexity of the terms in Eq. (4.20). We will examine these two cases—atom-dependent vs atom-independent grids—separately in what follows.

Before doing so, note that one can differentiate the identity $\mathbf{G}\mathbf{G}^{-1} = \mathbf{1}$ to obtain

$$(\mathbf{G}^{-1})^x = -\mathbf{G}^{-1}\mathbf{G}^x\mathbf{G}^{-1}. \tag{4.21}$$

In view of this, the derivative $(\mathbf{G}^{-1})^x$ in Eq. (4.20) is readily obtained once $\mathbf{G}^x$ is known, so only the latter is discussed herein.

1. Fixed grids

In this section, we limit our discussion to the case where the positions of the CHELPG grid points $\{\mathbf{r}_\alpha\}$ are independent of the positions of the nuclei. In the simplest case, this would mean a rectangular Cartesian grid, though the formalism presented below does not require the grid to be rectangular but simply independent of the locations of the QM nuclei. The *weights* of the grid points may or may not be independent of the nuclear positions, however. If all grid points are weighted uniformly ($w_\alpha = 1$), then terms involving the derivative of w_α will vanish, but we will not assume this to be the case. A non-uniform weighting scheme, in which $w_\alpha(\{\mathbf{r}_A\})$ is a function of the nuclear coordinates, has been used to ensure that the charges Q_A are smooth functions of molecular geometry despite the use of a Cartesian grid that is fixed in space.[28] We return to this point below.

The operator $\hat{\nabla}_A$ representing the vector derivative with respect to coordinates $\mathbf{r}_A = (x_A, y_A, z_A)$ is defined in Eq. (2.1). In what follows, we will use a simplified notation

$$f^{\nabla_A} \equiv \hat{\nabla}_A f \tag{4.22}$$

for the vector-valued gradient of a function $f(\mathbf{r}_A)$, with respect to the coordinates of nucleus A. Using this notation, the gradient of the matrix elements of $\mathbf{G}$ [Eq. (4.11)] is

$$G_{BC}^{\nabla_A} = \sum_\alpha^{N_{\text{grid}}} \left[\frac{w_\alpha^{\nabla_A}}{R_{\alpha B}\, R_{\alpha C}} + \left(\frac{\delta_{AB}}{R_{\alpha C}} + \frac{\delta_{AC}}{R_{\alpha B}} \right) \frac{w_\alpha \mathbf{R}_{\alpha A}}{R_{\alpha A}^3} \right]. \tag{4.23}$$

The first term in Eq. (4.23) vanishes if the weights are uniform, as in the traditional CHELPG procedure.[25,26] Inspired by other work on smooth discretization schemes,[85,86] however, we have previously considered a more sophisticated implementation,[28] in which switching functions are introduced in order to make sure that $w_\alpha(\{\mathbf{r}_A\})$ is a continuously differentiable function of the nuclear coordinates, despite the use of a fixed Cartesian grid to evaluate the electrostatic potential. In this approach, w_α is written as the product of a long-range weighting function w_α^{LR} and atomic switching functions $\{F_\alpha^A\}$,

$$w_\alpha(\mathbf{r}_\alpha, \{\mathbf{r}_A\}) = w_\alpha^{\text{LR}}(\mathbf{r}_\alpha, \{\mathbf{r}_A\}) \prod_A^{N_{\text{QM}}} F_\alpha^A(\mathbf{r}_\alpha, \mathbf{r}_A). \tag{4.24}$$

Gradients of Eq. (4.24) are straightforward,

$$\hat{\nabla}_A w_\alpha = \left(\hat{\nabla}_A w_\alpha^{\text{LR}}\right) \prod_B^{N_{\text{QM}}} F_\alpha^B + w_\alpha^{\text{LR}} \left(\hat{\nabla}_A F_\alpha^A\right) \prod_{B\neq A}^{N_{\text{QM}}} F_\alpha^B. \tag{4.25}$$

The switching functions are parameterized so that w_α is significantly different from zero only in the usual CHELPG fitting region, beginning at the atomic van der Waals radius and extending radially outward for a few Ångstroms. Correspondingly, $\hat{\nabla}_A w_\alpha \to 0$ as $\mathbf{r}_\alpha$ moves outside of this region. In terms of the switching function $\tau(R)$ that was defined in our previous work and used to construct the functions F_α^A,[28] this means that

$$\frac{\partial F_\alpha^A}{\partial x_A} = \left.\frac{\partial \tau}{\partial R}\right|_{R=R_{\alpha A}} \tag{4.26}$$

is only non-negligible when evaluated in regions where $\tau(R_{\alpha A})$ is non-negligible. See Appendix H of Ref. 22 for additional details.

Returning to the evaluation of Q_A^x in Eq. (4.20), we note that the derivative of $\mathbf{e}$ is more complicated as compared to that of $\mathbf{G}$, so we separate the former into pieces for convenience

$$e_B^{\nabla_A} = \Upsilon_{\nabla_A,B}^{(1)} + \Upsilon_{\nabla_A,B}^{(2)} + \Upsilon_{\nabla_A,B}^{(3)} + \Upsilon_{\nabla_A,B}^{(4)}. \tag{4.27}$$

The individual pieces can be read off term-by-term by inserting the definition of Φ_α [Eq. (4.5)] into the definition of $\mathbf{e}$ [Eq. (4.12)], then taking a derivative with respect to $\mathbf{r}_A$. They are,

$$\Upsilon_{\nabla_A,B}^{(1)} = \sum_\alpha \Phi_\alpha \left(\frac{w_\alpha}{R_{\alpha B}} \right)^{\nabla_A}, \tag{4.28a}$$

$$\Upsilon_{\nabla_A,B}^{(2)} = \sum_\alpha \frac{w_\alpha}{R_{\alpha B}} \left(\sum_C \frac{Z_C}{R_{\alpha C}} \right)^{\nabla_A}, \tag{4.28b}$$

$$\Upsilon_{\nabla_A,B}^{(3)} = -\sum_\alpha \frac{w_\alpha}{R_{\alpha B}} \sum_{\mu\nu} (\mathbf{I}_\alpha^{\nabla_A})_{\mu\nu} P_{\mu\nu}, \tag{4.28c}$$

$$\Upsilon_{\nabla_A,B}^{(4)} = -\sum_\alpha \frac{w_\alpha}{R_{\alpha B}} \sum_{\mu\nu} (\mathbf{I}_\alpha)_{\mu\nu} P_{\mu\nu}^{\nabla_A}. \tag{4.28d}$$

The first two terms involve only the positions of the nuclei and the CHELPG grid points, along with the precomputed values $\{\Phi_\alpha\}$ that were needed to compute the CHELPG charges in the first place. These terms can be simplified to obtain

$$\Upsilon_{\nabla_A,B}^{(1)} = \sum_\alpha \Phi_\alpha \left(\frac{w_\alpha^{\nabla_A}}{R_{\alpha B}} + \frac{w_\alpha \delta_{AB} \mathbf{R}_{\alpha A}}{R_{\alpha A}^3} \right) \tag{4.29}$$

and

$$\Upsilon_{\nabla_A,B}^{(2)} = \sum_\alpha \frac{w_\alpha Z_A \mathbf{R}_{\alpha A}}{R_{\alpha B} R_{\alpha A}^3}. \tag{4.30}$$

The term $\Upsilon_{\nabla_A,B}^{(3)}$ is the computational bottleneck since it involves derivatives of the electrostatic potential integrals,

$$\Upsilon_{\nabla_A,B}^{(3)} = -\sum_\alpha \frac{w_\alpha}{R_{\alpha B}} \sum_{\mu\nu} P_{\mu\nu} \left[\left\langle \mu^{\nabla_A} \middle| \frac{1}{\|\mathbf{r} - \mathbf{r}_\alpha\|} \middle| \nu \right\rangle + \left\langle \mu \middle| \frac{1}{\|\mathbf{r} - \mathbf{r}_\alpha\|} \middle| \nu^{\nabla_A} \right\rangle \right]. \tag{4.31}$$

Note that Eq. (4.31) does not contain a derivative of the operator $\|\mathbf{r} - \mathbf{r}_\alpha\|^{-1}$ because we have assumed that $\mathbf{r}_\alpha$ is independent of the position of nucleus A.

Finally there is $\Upsilon_{\nabla_A,B}^{(4)}$ in Eq. (4.27). Note from Eq. (4.28d) that this term explicitly involves the density matrix derivative $\partial P_{\mu\nu}/\partial x_A$, whereas the desired "$M$-derivatives" in Eqs. (3.15) and (3.18) are

Published under license by AIP Publishing

evaluated at fixed density matrix. As such, the contribution from $\Upsilon^{(4)}_{\nabla_A,B}$ is already included in the energy-weighted density matrix term in the gradient and should *not* be included here. With this in mind, we define

$$\widetilde{e}_B^{\nabla_A} = \Upsilon^{(1)}_{\nabla_A,B} + \Upsilon^{(2)}_{\nabla_A,B} + \Upsilon^{(3)}_{\nabla_A,B}. \tag{4.32}$$

Upon replacing $e_B^{\nabla_A}$ in Eq. (4.20) with $\widetilde{e}_B^{\nabla_A}$, the required M-derivative assumes the form

$$\sum_M \left(\frac{\partial Q_B}{\partial M}\right)\left(\frac{\partial M}{\partial x_A}\right) = \sum_{C,D}\Big[\widetilde{e}_C^{\nabla_A}\big(\mathbf{G}^{-1}\big)_{CD} + e_C\big(\mathbf{G}^{-1}\big)^{\nabla_A}_{CD} - (\lambda/2)\big(\mathbf{G}^{-1}\big)^{\nabla_A}_{CD}\Big](\delta_{BD} - \gamma_B). \tag{4.33}$$

The charge-response contribution $\Theta^{[x_A]}$ to the gradient [Eq. (3.18)] can now be assembled from Eq. (4.33) and the other equations derived in this section. Recall that the identity in Eq. (4.21) is used to obtain $(\mathbf{G}^{-1})^x$ from $\mathbf{G}^x$, the latter of which is provided in Eq. (4.23).

2. Atom-centered grids

Atom-dependent grids add another layer of complexity to the derivatives. We assume, as in our previous Lebedev grid-based implementation of the CHELPG charges,[21] that such grids consist of concentric atom-centered radial shells. In such a case, the locations of the grid points can be expressed as

$$\mathbf{r}_\alpha = \mathbf{r}_A + \mathbf{r}_{d,n}, \tag{4.34}$$

where the vector $\mathbf{r}_{d,n}$ comes from the Lebedev quadrature construction and depends upon the radial spacing (d) and the number of angular grid points (n) but is independent of the nuclear positions $\{\mathbf{r}_A\}$ and is therefore absent from the gradient expressions presented below.

The M-derivatives needed to evaluate $\Theta^{[x_A]}$ are still given by Eq. (4.33), just as in the fixed-grid case, but with modified forms of $\mathbf{G}^x$ and $\mathbf{e}^x$. For example, instead of $G^{\nabla_A}_{BC}$ as given in Eq. (4.23), for atom-centered grids the result is

$$G^{\nabla_A}_{BC} = \sum_\alpha \frac{w^{\nabla_A}_\alpha}{R_{\alpha B}R_{\alpha C}} + \sum_{\alpha\notin A}\left(\frac{\delta_{AB}}{R_{\alpha C}} + \frac{\delta_{AC}}{R_{\alpha B}}\right)\frac{w_\alpha \mathbf{R}_{\alpha A}}{R^3_{\alpha A}} - \sum_{\alpha\in A}\frac{w_\alpha(1-\delta_{BC})}{R_{\alpha B}R_{\alpha C}}\left(\frac{\mathbf{R}_{\alpha B}\delta_{AB}}{R^2_{\alpha B}} + \frac{\mathbf{R}_{\alpha C}\delta_{AC}}{R^2_{\alpha C}}\right). \tag{4.35}$$

The notation on the final sum ($\alpha \in A$) indicates that this summation should be performed over grid points $\mathbf{r}_\alpha$ whose origin lies on atom A, in the sense of Eq. (4.34). The notation $\alpha \notin A$ means the opposite, that grid points generated from atom A are excluded. In the first summation of Eq. (4.35), the grid point $\mathbf{r}_\alpha$ is unrestricted.

The terms $\Upsilon^{(1)}_{\nabla_A,B}$, $\Upsilon^{(2)}_{\nabla_A,B}$, and $\Upsilon^{(3)}_{\nabla_A,B}$ that define $\widetilde{e}_B^{\nabla_A}$ [Eq. (4.32)] are also modified for atom-centered grids, as follows. Equation (4.29) is replaced by

$$\Upsilon^{(1)}_{\nabla_A,B} = \sum_\alpha \frac{\Phi_\alpha w^{\nabla_A}_\alpha}{R_{\alpha B}} + \sum_{\alpha\notin A}\frac{\Phi_\alpha w_\alpha \mathbf{R}_{\alpha A}\delta_{AB}}{R^3_{\alpha A}} - \sum_{\alpha\in A}\frac{\Phi_\alpha w_\alpha \mathbf{R}_{\alpha B}(1-\delta_{AB})}{R^3_{\alpha B}}. \tag{4.36}$$

Equation (4.30) is replaced by

$$\Upsilon^{(2)}_{\nabla_A,B} = \sum_{\alpha\notin A}\frac{w_\alpha Z_A \mathbf{R}_{\alpha A}}{R_{\alpha B}R^3_{\alpha A}} - \sum_{\alpha\in A}\frac{w_\alpha}{R_{\alpha B}}\sum_C \frac{Z_C \mathbf{R}_{\alpha C}(1-\delta_{AC})}{R^3_{\alpha C}}. \tag{4.37}$$

Finally, Eq. (4.31) is replaced by

$$\Upsilon^{(3)}_{\nabla_A,B} = -\sum_\alpha \frac{w_\alpha}{R_{\alpha B}}\sum_{\mu\nu}P_{\mu\nu}\left[\left\langle \mu^{\nabla_A}\left|\frac{1}{\|\mathbf{r}-\mathbf{r}_\alpha\|}\right|\nu\right\rangle + \left\langle \mu\left|\frac{1}{\|\mathbf{r}-\mathbf{r}_\alpha\|}\right|\nu^{\nabla_A}\right\rangle - \left\langle \mu\left|\frac{1}{\|\mathbf{r}-\mathbf{r}_\alpha\|^3}\right|\nu\right\rangle\right]. \tag{4.38}$$

See Appendix H of Ref. 22 for additional details.

V. NUMERICAL APPLICATION

The QM/MM-Ewald method outlined above has been implemented in the Q-Chem electronic structure program,[87] where it has been available (with analytic gradients) since v. 4.4. The correctness of the analytic gradient was verified term-by-term using finite-difference calculations. Finite-difference derivatives $\partial\mathcal{E}/\partial x$ differ from our analytic gradient implementation by $\lesssim 10^{-7}$ a.u., if a five-point stencil is used with a step size of 0.001 Å. (Finite-difference results computed with a three-point stencil and displacements of ±0.001 Å sometimes differ from the analytic result by $\sim 10^{-5}$ a.u., even when tight thresholds are used.) We have also confirmed that numerical results from our own implementation of classical Ewald summation in Q-Chem match results obtained from the CHARMM program.[88]

In what follows, we describe the application of the new methodology to perform MD simulations of e^-(aq) in liquid water.

A. Ewald summation with net charge

Our simulations are carried out using a negatively charged unit cell, whereas the mathematical proof that the electrostatic sum defined in Eq. (2.4) can be converted into a pair of absolutely-convergent sums (a short-range one in real-space and another in reciprocal space) relies on charge neutrality in the unit cell.[8] This objection notwithstanding, we have in the past performed simulations of e^-(aq) using one-electron pseudopotential models combined with Ewald summation,[59,89,90] without apparent problems other than the fact that the vertical ionization energy (VIE) depends very strongly on the size of the periodic simulation cell.[89]

That said, a variety of classical MD studies have documented artifacts resulting from Ewald summation when the net charge is non-zero.[71,75,78,91–97] Let us set aside the utterly unsurprising result that there can be artifacts when $Q \neq 0$ and the simulation cell is small,[93,94] and consider what artifacts may remain even when the simulation cell is large. Issues with charged cells primarily manifest in the following cases: when mobile ions are present and the medium has a very inhomogeneous dielectric function (such as proteins or membranes in water, for example);[75] in calculations of the dielectric constant, which depends on fluctuations in the dipole moment of the simulation cell;[8,98] when the volume of the simulation cell is changed or else when the derivative of energy with respect to volume is required, as in a pressure calculation;[71,78] or when the overall charge Q is changed, as when the hydration free energy of an ion is computed via thermodynamic integration.[71,91–93,95,96]

Published under license by AIP Publishing

These problematic cases might have been anticipated from the nature of the charge correction E_{charge} in Eq. (2.19), which depends on both the overall charge Q and volume V of the simulation cell, and on the Ewald splitting parameter η. The charge correction shifts the electrostatic energy such that the Ewald potential averages to zero over the unit cell,[75,96,97] and *only* when it is included (and then only if both Q and V are fixed throughout the simulation) is the total electrostatic energy computed using Ewald summation independent of η.[77] Under conditions of fixed charge and volume, however, $\hat{\nabla}_i E_{\text{charge}} = \mathbf{0}$, consistent with a *uniform* background compensating charge density.[75] This is the case for the simulations presented here, which are primarily microcanonical.

It is indeed true for e^-(aq) that finite cell-size effects can have a dramatic influence (>1 eV) on the VIE, when Ewald summation is used in conjunction with a negatively charged unit cell.[89] (The manner in which continuum boundary conditions are implemented can have a similarly large effect in non-periodic calculations of the VIE.[89,90,99]) In the present work, we focus on structural rather than energetic aspects of electron solvation. Both the charge and the volume of the simulation cell are fixed, and the simulation cell is reasonably large (1024 water molecules). Ewald summation, with its implicit reliance on a compensating background charge,[6,9,10,13] mimicking an isotropic distribution of counter-ions when $Q \neq 0$,[75] seems appropriate for our purposes.

B. Simulation details

Previous simulations of e^-(aq) using cavity-forming pseudopotential models[89,100,101] predict spontaneous electron localization and subsequent cavity formation in <1 ps following injection of a delocalized electron into neat liquid water.[36] This is consistent with experimental estimates of the localization time scale.[102–104] Unfortunately, the presence of a QM/MM interface in our calculations makes it impossible to simulate the injection process directly because O–H moieties in the QM region that are hydrogen-bonded to MM water molecules will artificially stabilize the electron at the QM/MM interface, which lacks adequate Pauli repulsion interactions between the wave function and the MM water molecules. As such, our simulations are initiated using snapshots from a previous DFT-based QM/MM simulation of e^-(aq),[64] so the electron is initially localized in a pre-existing cavity. In previous work,[59] we demonstrated that pre-existing cavities immediately collapse in simulations using the non-cavity-forming pseudopotential model of Ref. 53, so the fact that a cavity is present at $t = 0$ is certainly no guarantee that it will persist.

The QM region in our simulations consists of the 24 H_2O molecules that lie within a radius of 5.5 Å of the centroid of the spin density, for the DFT-based trajectory data obtained from Ref. 64. The full, periodic simulation cell contains 1024 water molecules with $L = 31.3192$ Å, affording a bulk water density of 0.997 g/cm^3. Simulations were propagated under conditions of constant energy using the velocity Verlet algorithm with a time step of 42 a.u. (= 1.016 fs), consistent with the fact that all water molecules were treated as fully flexible. Initial nuclear velocities were selected at random from a Maxwell-Boltzmann distribution characteristic of $T = 300$ K. MM water molecules were described using the modified TIP3P water model that is part of the CHARMM27 force field.[105] In principle, one probably ought to re-optimize the MM Lennard-Jones parameters for use in QM/MM calculations,[106–108] but we have not done so here. This is probably justified over the short time scales of the simulations reported here.

We use different Ewald splitting parameters for the MM-MM and QM-MM interactions, as described in Ref. 21 and in Appendix D of Ref. 22. Setting

$$C = \sqrt{-\ln(\tau_{\text{SCF}}/E_{\text{h}})}, \tag{5.1}$$

where $\tau_{\text{SCF}} = 10^{-8}\ E_{\text{h}}$ is the SCF convergence threshold, we set $\eta_{\text{MM}} = 2C/L \approx 0.274$ Å^{-1} for the MM-MM interactions. For the QM-MM interactions, the optimal value η_{QM} is obtained as a root of the equation

$$\frac{2CL^3\eta_{\text{QM}}^3}{\pi^{3/2}} + \frac{L^2\eta_{\text{QM}}^2}{\pi^{1/2}} - L\eta_{\text{QM}} - 2C = 0. \tag{5.2}$$

For C and L as described above, the solution is $\eta_{\text{QM}} \approx 0.06$ Å^{-1}.

The QM region, consisting of $(H_2O)_{24}^-$, is described at the HF+D3/3-21++G* level, meaning Hartree-Fock (HF) theory combined with Grimme's third-generation "D3" empirical dispersion potential.[109] To avoid energy drift caused by violation of time-reversal symmetry,[110] the SCF guess is regenerated at every time step from a superposition of atomic densities.

Regarding the choice of basis set, we have previously shown that a single set of atom-centered diffuse functions is sufficient to support a cavity-bound electron in the condensed phase.[61,111] (Such a basis set is *not* adequate for gas-phase hydrated-electron clusters, where additional diffuse functions are necessary to avoid artifacts.[68,112]) Even so, the use of diffuse basis functions significantly increases the cost of the calculations by muting the effectiveness of integral thresholding.

That said, the present calculations provide an excellent test to verify that our CHELPG-based QM/MM-Ewald procedure is applicable to arbitrary basis sets. Both Mulliken and Löwdin charges are badly behaved in the presence of diffuse functions, and while that fact is widely known, the presence of $\partial Q_A/\partial P_{\mu\nu}$ in the Fock matrix [Eq. (2.27)] makes this far more problematic than simply obtaining charges $\{Q_A\}$ whose values are non-intuitive and basis-set dependent. In our experience, use of Mulliken or Löwdin charges in the QM/MM-Ewald procedure[21] (and the related "XPol" method[27,28,113,114]) often leads to SCF convergence failure when diffuse basis functions are employed. In contrast, we have encountered no such problems with CHELPG charges. For the calculations reported here, the Q_A are CHELPG charges computed using atom-centered Lebedev grids with 50 angular grid points per radial shell, with radial shells that begin at the atomic van der Waals radius of each atom and extend outward for another 3.0 Å, in 0.5 Å intervals.

Calculation of the requisite charge derivatives $\partial Q_A/\partial P_{\mu\nu}$ does incur significant computational expense when CHELPG charges are used, as is clear from the timing data presented in Table I. As compared to a QM/MM simulation without periodic boundary conditions, the QM/MM-Ewald simulations are about six times more expensive, with most of the increased cost incurred by the aforementioned charge-derivative contributions to the gradient. We are currently working to reduce this cost.

C. Results

The QM region used in these simulations contains approximately two solvation shells around the centroid of the spin density.

Published under license by AIP Publishing

TABLE I. Average timings for a single MD time step, for HF+D3/3-21++G* simulations of e^-(aq) with 24 QM and 1000 MM water molecules in the simulation cell. The data labeled "QM/MM" represent non-periodic calculations with the same simulation cell, so comparison to the QM/MM-Ewald timings demonstrates the cost of the periodic boundary conditions. All calculations were parallelized over 20 cores on a single compute node, with thresholds and CHELPG grid parameters as described in the text. The SCF energy and gradient timings contain all of the QM/MM terms in addition to the purely QM part.

	Time per MD step[a] (s)			
	QM/MM		QM/MM-Ewald	
	Wall	CPU	Wall	CPU
MM energy	0.2	3.9	1.0	19.4
MM gradient	0.3	0.3	0.7	13.4
SCF energy	26.5	523.7	59.5	1057.1
SCF gradient	9.1	99.7	106.2	1373.6
Total[b]	41.2	661.8	172.8	2507.1

[a]Dell PowerEdge C6420 server, 2.4 GHz Intel Xeon 6148 Skylake processor.
[b]Total time per step is slightly larger than the combined energy + gradient time, due to minor additional overhead.

In general, this sort of QM/MM simulation of an aqueous solute, in which certain solvent molecules are included in the QM region, is bound to be problematic over sufficiently long time scales because the mean residence time of a water molecule in the first solvation shell is rather short, e.g., $\lesssim$13 ps for I^-(aq),[115–118] which has a cavity size similar to that of e^-(aq). The trajectories reported here are at most 5 ps in length, however, so what is more problematic is the very rapid diffusion of e^-(aq), which occurs via librational motions of the water molecules.[36] One solution would be to use an "adaptive" QM/MM procedure,[119] in which solvent molecules are allowed to transition smoothly (but dynamically) between the QM and MM regions. Such methods are both technically and computationally more involved, however, and are not implemented in our code. Alternatively, a confining potential can be used when only structural or thermodynamic (rather than dynamical) information is of interest,[120] but given the controversy surrounding the structure of e^-(aq), we prefer not to complicate the issue in this way.

As a result, we must live with the fact that any room-temperature trajectory in which e^-(aq) is cavity-centered (at $t = 0$) in a QM region with a radius of 5.5 Å will evolve, within a few picoseconds, to one where the spin density resides near the QM/MM interface. At that point, the trajectory in question is no longer usable or interpretable. We can easily monitor this evolution since our code sets the coordinate origin at each time step to be equal to the center of mass of the QM nuclei. Let r_0 denote the distance between this coordinate origin and the centroid of the spin density, defined as

$$\rho_{\text{spin}}(\mathbf{r}) = \rho_\alpha(\mathbf{r}) - \rho_\beta(\mathbf{r}). \tag{5.3}$$

The quantity $r_0(t)$ monitors the drift of the unpaired electron away from the center of the QM region. Meanwhile the radius of gyration of the spin density (r_{gyr}), which is defined by the equation

$$r_{\text{gyr}}^2 = \left\langle \|\mathbf{r} - \langle\mathbf{r}\rangle\|^2 \right\rangle = \int \left(r^2 - \langle\mathbf{r}\rangle \cdot \langle\mathbf{r}\rangle\right)\rho_{\text{spin}}(\mathbf{r})\, d\mathbf{r}, \tag{5.4}$$

provides a measure of the size of the electron. The quantity $r_0(t) + r_{\text{gyr}}(t)$ then reports on how the position of the outer edge of the spin density evolves with time. When $r_0(t) + r_{\text{gyr}}(t)$ reaches values approaching 5.5 Å, the trajectory is no longer usable.

As an example, Fig. 2 plots $r_0(t) + r_{\text{gyr}}(t)$ for two different trajectories. In one of these, the spin density begins to migrate away from the center of the QM region starting around $t \approx 1.0$ ps, and by $t \approx 1.5$ ps, it has breached the QM/MM interface, which is evident upon examination of the spin density. The time propagation is halted at this point, as this particular trajectory is no longer usable. In contrast, for the second trajectory depicted in Fig. 2 the quantity $r_0(t) + r_{\text{gyr}}(t)$ only once goes above 5.0 Å (briefly, around $t \approx 3.6$ ps), and stays under 5.5 Å for the entire 5 ps of dynamics. This means that $\rho_{\text{spin}}(\mathbf{r})$ remains safely within the QM region over this entire trajectory, as is evident from the plot of $\rho_{\text{spin}}(\mathbf{r})$ at $t = 5$ ps that is depicted in Fig. 2. Notably, even in trajectories that migrate quickly to the QM/MM boundary, we do not observe any collapse of the excluded volume that is present at $t = 0$.

The longer of the two trajectories plotted in Fig. 2, during which $\rho_{\text{spin}}(\mathbf{r})$ remains within the QM region for the full 5 ps of time propagation, is used for all subsequent analysis. Figure 3 shows a close-up view of $\rho_{\text{spin}}(\mathbf{r})$ at the end of this trajectory. As is typical for this system, the spin density closely resembles the singly-occupied molecular orbital (SOMO). As reported elsewhere,[61,111] a basis set with only a single set of atom-centered diffuse functions clearly has no difficulty describing a SOMO that is not associated with any particular water molecule but instead inhabits a void in the solvent.

Figure 4 demonstrates stable energy conservation, albeit with a slight drift following the initial equilibration period in which the system is mostly adjusting to the change in force field with respect

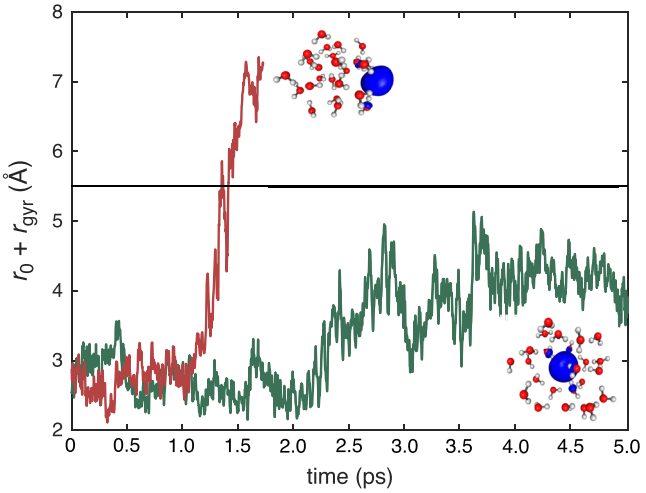

FIG. 2. Time evolution of the quantity $r_0(t) + r_{\text{gyr}}(t)$ for two different trajectories, with snapshots depicting the spin density $\rho_{\text{spin}}(\mathbf{r})$ at the ending point of each. The quantity r_{gyr} is the radius of gyration of $\rho_{\text{spin}}(\mathbf{r})$ [Eq. (5.4)], and r_0 is the distance between the centroid of $\rho_{\text{spin}}(\mathbf{r})$ and the center of mass of the QM region. The quantity $r_0(t) + r_{\text{gyr}}(t)$ thus measures the time evolution of the "edge" of the spin density as compared to the center of the QM region. Once this quantity reaches 5.5 Å (the initial radius of the QM region, indicated by a horizontal line), the trajectory is no longer usable.

Published under license by AIP Publishing

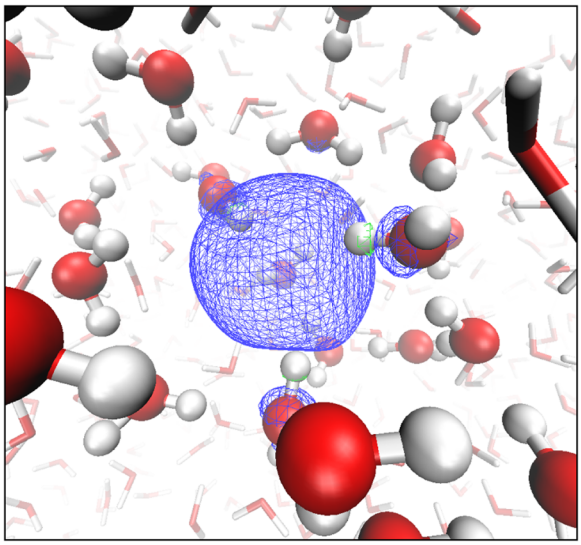

FIG. 3. Spin density of e^-(aq) at the conclusion (t = 5 ps) of the longer trajectory shown in Fig. 2. The QM water molecules are shown in a ball-and-stick representation and the MM water molecules in a tubular representation. The isocontour that is plotted (ρ_{spin} = ±0.0015 a.u.) encompasses 92% of $\rho_{spin}(\mathbf{r})$. Extremely small regions of green mesh indicate where $\rho_{spin}(\mathbf{r}) < 0$; these regions are confined to the O–H moieties that are coordinated directly to e^-(aq).

to that used in Ref. 64. The rate of drift is slightly larger than what is typically observed in Born-Oppenheimer MD simulations,[121] consistent with our larger time step of 42 a.u. (1.016 fs) as compared to the more standard value of 20 a.u. (0.484 fs).[121–123] Short

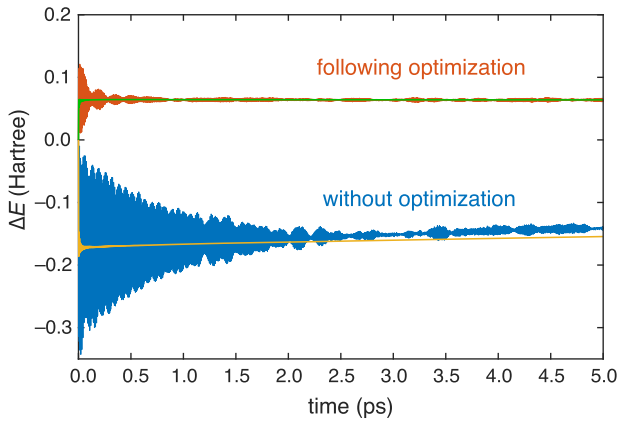

FIG. 4. Energy fluctuations ΔE over the course of a trajectory initialized either with or without prior geometry optimization. In either case, the running average of the energy (relative to its value at t = 0) is plotted as well. The non-optimized trajectory corresponds to the longer of the two trajectories plotted in Fig. 2, for which the initial geometry was taken directly from Ref. 64. The standard deviation in ΔE over this 5 ps trajectory is σ = 0.031514 E_h in a total energy whose time-averaged value is $\langle E \rangle$ = −1823.738097 E_h. For the optimized case, we took the same snapshot from Ref. 64 but performed 128 optimization steps (at the QM/MM level of theory described here) prior to beginning the MD trajectory. In this case, we obtain σ = 0.004681 E_h and $\langle E \rangle$ = −1831.978635 E_h.

trajectories run with Δt = 21 a.u. exhibit much smaller energy fluctuations; see Fig. S3 in the supplementary material. This is consistent with very large initial velocities arising from the change in water force field, as discussed in the supplementary material.

Figure 4 also demonstrates that much smaller energy fluctuations are obtained if the geometry is first relaxed at the QM/MM level of theory that is used for the subsequent MD simulation, rather than simply starting from the structure obtained from Ref. 64. Geometry optimization lowers the total energy by ≈8.8 E_h, nearly all of which comes from relaxing the bond-stretching terms in the water force field. This relaxation eliminates the energy drift in the subsequent MD simulation (see Fig. 4), meaning that the drift that we observe starting from an unrelaxed geometry would likely disappear upon further equilibration of the simulation. The lack of pre-equilibration, however, does mean that we may effectively be operating well above T = 300 K in these simulations, since the system is initialized with significant energy in the classical O–H bonds. Despite the elevated temperature, a well-defined cavity persists in every trajectory that we have examined.

Even with the larger time step of Δt = 42 a.u. and lack of pre-equilibration in the trajectory of Fig. 4, the overall energy drift is small. Defining relative fluctuations

$$\delta(t) = \frac{E(t) - E(0)}{E(0)}, \tag{5.5}$$

the drift amounts to only $\langle \delta \rangle = 1.36 \times 10^{-5}$ when averaged over the whole trajectory. Use of Cartesian grids vs atom-centered Lebedev grids to compute the CHELPG charges makes essentially no difference (see Fig. S4), although the Lebedev grids are vastly more efficient. The Lebedev grid parameters specified here (Δr = 0.5 Å and r_{max} = 3.0 Å) result in ≈850 grid points for the electrostatic potential fitting, vs ≈60 000 in the case of a regular Cartesian grid with a comparable spacing (Δx = 0.5 Å) and radial extent.

It is clear from Figs. 2 and 4 that the first 2 ps of dynamics in our 5 ps trajectory constitutes an equilibration period. In terms of impact on the total energy, the primary result of this equilibration is readjustment of the bond lengths of the classical water molecules. Around the time that the energy fluctuations stabilize (t ≈ 2.0–2.5 ps), one can observe a pronounced shift in the value of $r_0(t)$; see Fig. 5(a). This indicates that the center of the spin density has stabilized in a location (r_0 ≈ 2 Å) that is not quite at the center of the QM region, the latter of which defines r_0 = 0. At the same time, the *size* of the spin density, as measured by r_{gyr}, fluctuates about its mean value $\langle r_{gyr} \rangle$ = 2.15 Å essentially from the outset of the simulation; see Fig. 5(b). It is evident from Fig. 2, which depicts the same trajectory, that the sum $r_0(t) + r_{gyr}(t)$ remains well within the 5.5 Å radius of the QM region.

Several isosurface plots of $\rho_{spin}(\mathbf{r})$ along this trajectory are presented in Fig. 6. These snapshots demonstrate that the excluded volume from which water molecules are expelled remains stable both during and after the initial equilibration period of ~2 ps. In fact, there is really no qualitative change in $\rho_{spin}(\mathbf{r})$ even with respect to the initial, unrelaxed snapshot taken at t = 0, where the cavity comes from a separate DFT-based QM/MM simulation using a rather different computational approach.[64] The cavity remains stable through the end of the trajectory at t = 5 ps. It is also stable (for at least several

Published under license by AIP Publishing

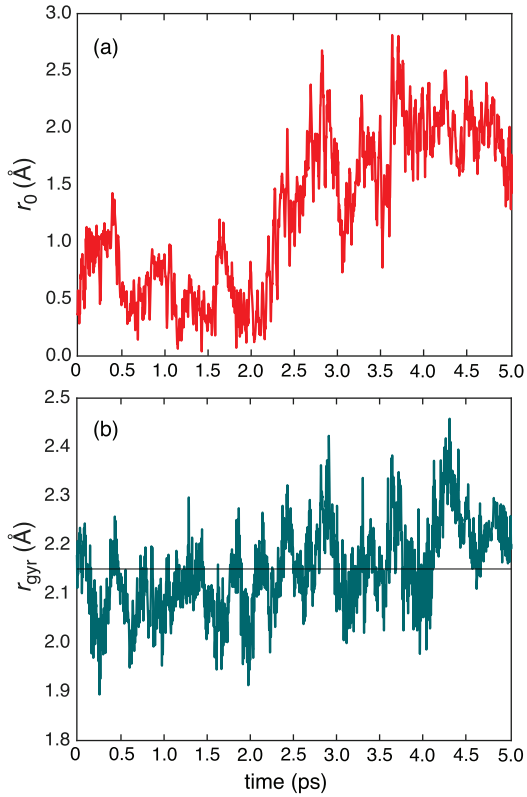

FIG. 5. Plots of (a) the distance r_0 between the centroid of $\rho_{spin}(\mathbf{r})$ and the center of mass of the QM region, and (b) the radius of gyration of $\rho_{spin}(\mathbf{r})$. The horizontal line in (b) indicates the average value, $\langle r_{gyr} \rangle$ = 2.15 Å. These data are taken from the non-optimized trajectory whose energy fluctuations are plotted in Fig. 4, which is also the 5 ps trajectory from Fig. 2.

more picoseconds) if we spontaneously switch the level of theory to B3LYP+D3/3-21++G* and simultaneously switch from propagation at constant energy to propagation at constant temperature, enforced using a Nosé-Hoover thermostat[124] set at T = 300 K. Spin densities

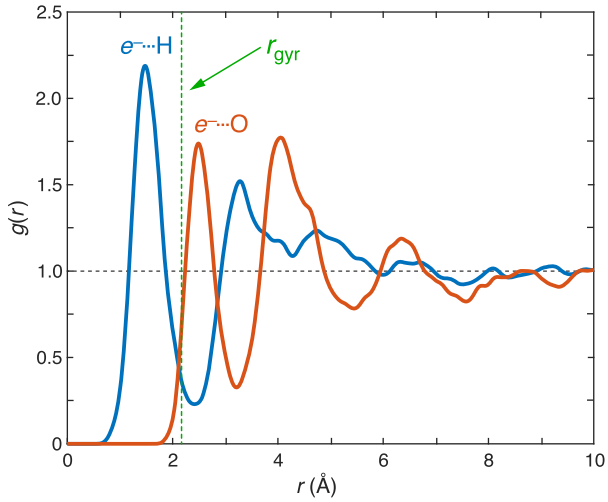

FIG. 7. Radial distribution functions (RDFs) for $e^- \cdots$ O and $e^- \cdots$ H, where the electron coordinate is the centroid of $\rho_{spin}(\mathbf{r})$. Both RDFs were computed from a single 5 ps trajectory and were smoothed with a Gaussian windowing function whose width is 0.055 Å for $e^- \cdots$ O and 0.090 Å for $e^- \cdots$ H. The ensemble-averaged radius of gyration, $\langle r_{gyr} \rangle$ = 2.15 Å, is also indicated.

from this B3LYP+D3 simulation are depicted in the lower part of Fig. 6.

Returning to the constant-energy HF+D3 trajectory, further evidence of the cavity-bound nature of the spin density comes in the form of radial distribution functions (RDFs) $g(r)$ for the $e^- \cdots$ H and $e^- \cdots$ O coordinates (Fig. 7), which demonstrate that hydrogen atoms are completely excluded for $r \lesssim 0.7$ Å, and oxygen atoms for $r \lesssim 1.8$ Å. This also affirms the coordination motif that is suggested in Fig. 3, and found in many other theoretical studies,[36] in which a single O–H moiety from each water molecule is coordinated to the electron's charge cloud. This is also the coordination motif that has been inferred from resonance Raman studies of e^-(aq) in mixtures of H_2O and D_2O.[125]

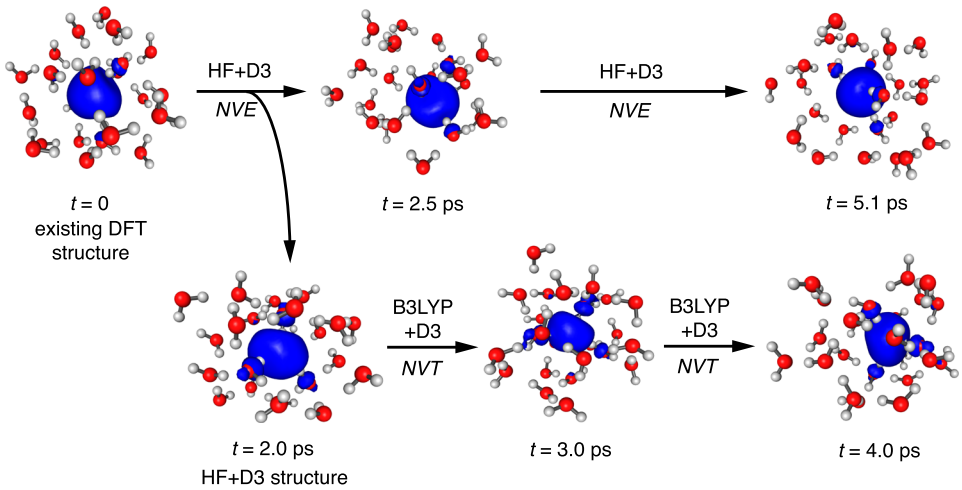

FIG. 6. Time evolution of $\rho_{spin}(\mathbf{r})$ showing only the QM water molecules in each snapshot. The upper trajectory, labeled "HF+D3," corresponds to the trajectory of Fig. 5. In an accompanying calculation, the level of theory was spontaneously switched to B3LYP+D3 at t = 2.0 ps, and the constant-energy (*NVE*) time propagation switched to constant-temperature (*NVT*) propagation at the same time. The result is shown in the lower part of the figure. Spin density isosurfaces closely resemble those of the singly-occupied molecular orbital (SOMO). They are plotted using an isosurface value of 0.002 a.u. that encompasses >90% of $\rho_{spin}(\mathbf{r})$.

Published under license by AIP Publishing

These RDFs were computed by averaging over the 5 ps duration of the trajectory, taking the position of the electron to be the centroid of $\rho_{\text{spin}}(\mathbf{r})$. RDFs obtained from a 1 ps trajectory whose structure was relaxed prior to the MD simulation exhibit a somewhat more well-defined cavity structure as compared to those in Fig. 7, in the sense that the peaks in the RDF are narrower and $g(r)$ goes completely to zero in between its first and second maxima, unlike the RDFs shown in Fig. 7. (See Fig. S2 in the supplementary material for a comparison of RDFs obtained for these two trajectories.) Both trajectories exhibit well-defined first and second local maxima in both the $e^-\cdots$ H and $e^-\cdots$ O RDFs, and these maxima occur at precisely the same values of r in both trajectories. This supports our contention that the initial ~2 ps of equilibration in our 5 ps trajectory does not substantially bias the resulting structure.

In view of the average radius of gyration that we obtain for the 5 ps trajectory, $\langle r_{\text{gyr}}\rangle$ = 2.15 Å, essentially the entire first peak in the $e^-\cdots$ H RDF is contained inside of the spin density, although very little of the first peak in the $e^-\cdots$ O $g(r)$ lies within this radius. As we have argued for some time,[36,89,126,127] the spin density of e^-(aq) penetrates into the second solvation shell of water molecules, even for cavity-bound structures. This behavior is seen even in one-electron pseudopotential models,[89] where it can be characterized either in structural terms (changes in the average number of hydrogen bonds per water molecule that disappear only in the third solvation shell) or in dynamical terms (autocorrelation functions for H_2O librational dynamics that return to bulk-like behavior only in the third solvation shell). A detailed analysis of these metrics can be found in Ref. 89. Penetration of $\rho_{\text{spin}}(\mathbf{r})$ beyond the excluded-volume region is by no means limited to many-electron (e.g., DFT) descriptions of e^-(aq), as has sometimes been erroneously suggested.

The first maxima in the two RDFs shown in Fig. 7 occur at ≈1.5 Å for $e^-\cdots$ H and at ≈2.5 Å for $e^-\cdots$ O. These distances are ≈0.5 Å smaller than those obtained in bulk water simulations using the cavity-forming pseudopotential model of Turi and Borgis,[101] but much closer to the values obtained using the cavity-forming pseudopotential model of Jacobson and Herbert.[89] (Both models were parameterized in much the same way, but the Jacobson-Herbert model uses a polarizable force field for water, whereas the Turis-Borgis model uses a fixed-charge force field.) A comparison of the RDFs obtained from both of these pseudopotential models, alongside those obtained from the non-cavity-forming pseudopotential model of Schwartz and co-workers,[53] can be found in Ref. 61. RDFs obtained in the present work, and in that of Jacobson and Herbert,[89] agree reasonably well with DFT results from Uhlig *et al.*[64]

Figure 8 plots the time-dependent Hartree-Fock eigenvalues for several of the frontier MOs. The quantity $-\epsilon_{\text{SOMO}}(t)$ is the Koopmans' approximation to the time-dependent vertical ionization energy (VIE), and the present simulations afford a time-averaged Koopmans' VIE of 2.96 ± 0.42 eV. Considering that the accuracy limits of Koopmans' theorem are ~0.5 eV at best,[68,128] this is at least qualitatively consistent with the most recent experimental value of VIE = 3.7 ± 0.1 eV for e^-(aq).[129] It should also be noted that long-range polarization effects—well beyond the 24 QM water molecules used here—are extremely important to obtaining a converged VIE.[89,90,99] Notably, we have previously computed an accurate *ab initio* VIE of 3.75 eV taking snapshots from a DFT/MM simulation of e^-(aq) then computing the VIE at the MP2 level along with a careful treatment of continuum boundary conditions.[99]

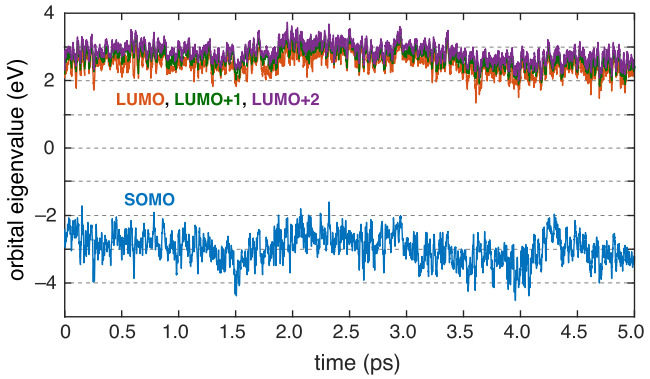

FIG. 8. Time-dependent fluctuations in the Hartree-Fock eigenvalues for the frontier MOs, for the trajectory analyzed in Figs. 4 and 5.

D. Discussion

In contrast to the stable cavities that are observed in our simulations, a pre-existing cavity immediately collapses in simulations performed using the non-cavity pseudopotential model developed by Larsen, Glover, and Schwartz (LGS).[53] This is true even for *geometry optimization*, that is, even at T = 0.[59] The resulting RDFs exhibit very little structure, and the value of $g(r)$ at r = 0 is considerably different from zero,[61] in sharp contrast to the RDFs for cavity-forming models. The latter are exemplified by those shown in Fig. 7. The present results strongly suggest that Hartree-Fock theory alone is sufficient to stabilize an excluded-volume structure.

This is interesting in view of the fact that the LGS electron–water pseudopotential was actually parameterized using Hartree-Fock theory,[53] as was an alternative, *cavity-forming* pseudopotential developed by Turi *et al.*[51,101] that was mentioned above. Both Turi *et al.*[51] and Larsen *et al.*[53] perform a "static exchange" Hartree-Fock (SE-HF) calculation on $(H_2O)^-$ contained within a confining potential, which is necessary because the anion of a single water molecule is unbound. Within the SE-HF approximation, the molecular orbitals of H_2O are frozen and only the lowest unoccupied molecular orbital (LUMO) is optimized self-consistently.[51,89,130–132] (Relaxing the H_2O molecular orbitals amounts to the incorporation of electron–water polarization interactions, and the intention is to include these separately, by means of an *ad hoc* polarization potential.[89,131,132]) Because the SE-HF calculation contains only a single active electron, the pseudopotential is not uniquely defined, but this ambiguity is removed by an additional constraint of kinetic energy minimization.[130] The outcome of this procedure is a pseudo-orbital that is free of the LUMO's large oscillations in the core molecular region but matches the LUMO asymptotically (at large electron–molecule separation), and which reproduces exactly the same eigenvalue, ϵ_{LUMO}.[51,89,130]

As a final step, the real-space potential corresponding to this pseudo-orbital is computed on a grid and fit to an analytic potential for use in simulations.[53,89,101] It appears, however, that the

Published under license by AIP Publishing

qualitative outcome of these simulations is sensitive to very subtle details in the fitting procedure.[59] Of three pseudopotential models developed so far based on SE-HF and related calculations for $(H_2O)^-$,[53,89,101] two of them predict spontaneous cavity formation in bulk water.[89,101] The LGS pseudopotential is the exception, and we note that Larsen *et al.* do make use of a smoothing procedure in order to eliminate high-momentum components of the potential.[53] (This reduces the cost of subsequent grid-based QM/MM simulations.)

Simulations reported here suggest that the fitting procedure used to construct the LGS pseudopotential may not be faithful to the underlying Hartree-Fock model. Similar concerns have been raised by Turi *et al.*,[52,132] albeit on entirely different grounds. In particular, in Ref. 52 it was noted that the ground-state eigenvalue of the LGS model Hamiltonian (ϵ_{LGS}) is smaller than the pseudo-orbital eigenvalue computing using *only* the confining potential, without a water molecule present at all: $\epsilon_{\mathrm{LGS}} < \epsilon_{\mathrm{conf}}$. The LGS electron–water pseudopotential therefore stabilizes the electron with respect to the background confining potential. In reality, however, the SE-HF pseudo-orbital eigenvalue for $(H_2O)^-$ in a confining potential ($\epsilon_{\mathrm{SE\text{-}HF+conf}}$) is known to be *larger* than the eigenvalue obtained using the confining potential alone,[52]

$$\epsilon_{\mathrm{LGS}} < \epsilon_{\mathrm{conf}} < \epsilon_{\mathrm{SE\text{-}HF+conf}}. \tag{5.6}$$

The inequality $\epsilon_{\mathrm{conf}} < \epsilon_{\mathrm{SE\text{-}HF+conf}}$ indicates that the electron–water interaction potential is net repulsive within the SE-HF model. In other words, when averaged over all of three-dimensional space, the presence of the H_2O molecule in the one-electron SE-HF calculation *raises* the energy, relative to that of a single electron trapped in the confining potential alone. This is true despite the fact that there certainly exist regions of space around a water molecule that are highly favorable to an electron, e.g., near the hydrogen atoms at the positive end of the O–H bond dipoles.

The fact that $\epsilon_{\mathrm{LGS}} < \epsilon_{\mathrm{conf}}$ means that the LGS interaction potential for $(H_2O)^-$ *lowers* rather than *raises* the energy of the electron, relative to the bare confining potential. The LGS pseudopotential is net attractive rather than net repulsive, attributable to fitting errors that render the LGS potential overly attractive near the hydrogen atoms.[132] This provides a means to understand the collapse of the cavity in the LGS model vs its persistence in other one-electron models, and importantly, its persistence in Hartree-Fock theory itself, as evidenced by the simulations presented here. Simulations with several slightly modified versions of the LGS potential actually *do* predict spontaneous cavity formation,[52,56,59] suggesting that this interaction potential lies on the cusp of being cavity-forming or not, depending on small details.

VI. CONCLUSION

We have formulated and implemented analytic energy gradients for a robust version of the QM/MM-Ewald method that uses CHELPG atomic charges rather than Mulliken charges to represent the periodic images of the QM region. This facilitates QM/MM calculations with periodic boundary conditions based on proper Ewald summation rather than with cutoffs or minimum-image convention. The procedure maintains the variational nature of the SCF description of the QM region and works for arbitrary basis sets, as demonstrated here with simulations involving a plethora of diffuse basis functions. We have implemented the QM/MM-Ewald method for both Hartree-Fock and DFT descriptions of the QM region. Correlated wave function calculations are also possible using CHELPG charges computed from the Hartree-Fock density.

Calculation of CHELPG charges does require evaluation of the electrostatic potential on a real-space grid. By itself this is rather trivial, but to compute the analytic gradient of the QM/MM-Ewald energy requires *derivatives* of the electrostatic potential integrals, evaluated at the same set of grid points. Despite the fact that these are one-electron integrals, this can create a significant bottleneck. (In fact, even the derivatives $\partial Q_A/\partial P_{\mu\nu}$ that are needed to construct the Fock matrix for single-point energy calculations can constitute a significant bottleneck when the QM region is large.[35]) The cost is considerably reduced using a version of the CHELPG procedure based on atom-centered Lebedev grids,[21] rather than the Cartesian grids used in the original CHELPG procedure.[25,26] Nevertheless, this remains a major computational bottleneck and work is currently underway to reduce this cost.

As a rigorous test of the method, we presented MD simulations of the aqueous electron at the HF+D3/3-21++G* level, using a QM region consisting of $(H_2O)_{24}^-$ in a large box of classical water molecules at $T = 300$ K. Starting from existing DFT-based QM/MM trajectories,[64] we find that "cavity-bound" structures of e^-(aq) are stable on a time scale of at least 5 ps at the HF+D3/3-21++G* level. Preliminary calculations at the B3LYP+D3 level do not change this result in a qualitative way. Simulation of longer time scales is limited by rapid diffusion of e^-(aq), which will require either a significantly larger QM region or else adaptive QM/MM boundary conditions.[119] However, despite the relatively short time scales examined here, our results are entirely consistent with the idea that the electron–water interaction potential is net repulsive[52] and that e^-(aq) occupies an excluded volume in the structure of liquid water.

Historically, studies of electron localization in polar fluids considered two competing paradigms to describe the transition from a delocalized, quasi-free electron in the conduction band to a localized species e^-(aq).[102,133–137] The question posed in the early literature was one of whether the electron is "trap-seeking" or "trap-digging." It has since been established that the structure of liquid water and simple alcohols contain pre-existing "traps" that facilitate the initial steps of electron localization.[136–139] These are instantaneous defects in the liquid structure, where dangling O–H moieties created by transiently broken hydrogen bonds expose the attractive parts of the electron–water interaction potential, facilitating formation of what has sometimes been called the "pre-solvated" or "wet" electron.[103,140–146] This has been observed in some calculations,[104] and the results presented here are not inconsistent with that picture, although we have not attempted to simulate the initial steps of electron localization. At the same time, however, the often-overlooked net repulsive nature of the electron–water interaction potential should be considered.[52] This suggests that the solvated electron quickly transitions from a trap-seeker to a trap-digger, where the hydrogen-bond network rearranges to accommodate the electron and the overall repulsive nature of the electron–water interaction takes over, pushing out water molecules to form an excluded volume during the transition from the initial pre-solvated state to the final, thermalized species, e^-(aq). Our simulations are the first to make extensive use of diffuse basis functions, yet nowhere do we find evidence for a non-cavity species. Recent, fully QM

Published under license by AIP Publishing

ab initio MD simulations also support the cavity-bound picture of this species.[66,147]

SUPPLEMENTARY MATERIAL

See the supplementary material for additional simulation data related to the choice of time step, energy conservation, and equilibration.

ACKNOWLEDGMENTS

We thank Professor Yihan Shao (University of Oklahoma) and Professor Lee Woodcock (University of South Florida) for checking results from our implementation of Ewald summation in Q-Chem against those obtained using the CHARMM program,[88] via the Q-Chem/CHARMM interface.[148] This work was supported by the National Science Foundation under Grant Nos. CHE-0748448 and CHE-1300603. Calculations were performed at the Ohio Supercomputer Center under Project No. PAA-0003.[149] J.M.H. is a fellow of the Alexander von Humboldt Foundation and serves on the Board of Directors of Q-Chem, Inc.

REFERENCES

[1]H. Schreiber and O. Steinhauser, "Cutoff size does strongly influence molecular dynamics results on solvated polypeptides," Biochemistry **31**, 5856–5860 (1992).
[2]D. M. York, T. A. Darden, and L. G. Pedersen, "The effect of long-range electrostatic interactions in simulations of macromolecular crystals: A comparison of Ewald and truncated list methods," J. Chem. Phys. **99**, 8345–8348 (1993).
[3]D. M. York, A. Wlodawer, L. G. Pedersen, and T. A. Darden, "Atomic-level accuracy in simulations of large protein crystals," Proc. Natl. Acad. Sci. U. S. A. **91**, 8715–8718 (1994).
[4]D. M. York, W. Yang, H. Lee, T. Darden, and L. G. Pedersen, "Toward the accurate modeling of DNA: The importance of long-range electrostatics," J. Am. Chem. Soc. **117**, 5001–5002 (1995).
[5]J. E. Roberts and J. Schnitker, "Boundary conditions in simulations of aqueous ionic systems: A systematic study," J. Phys. Chem. **99**, 1322–1331 (1995).
[6]M. P. Tosi, "Cohesion of ionic solids in the Born model," Solid State Phys. **16**, 1–120 (1964).
[7]A. Redlack and J. Grindlay, "Coulombic potential lattice sums," J. Phys. Chem. Solids **36**, 73–82 (1975).
[8]S. W. de Leeuw, J. W. Perram, and E. R. Smith, "Simulation of electrostatic systems in periodic boundary conditions. I. Lattice sums and dielectric constants," Proc. R. Soc. London, Ser. A **373**, 27–56 (1980).
[9]A. Y. Toukmaji and J. A. Board, Jr., "Ewald summation techniques in perspective: A survey," Comput. Phys. Commun. **95**, 73–92 (1996).
[10]P. Gibbon and G. Sutmann, "Long-range interactions in many-particle simulation," in *Quantum Simulations of Complex Many-Body Systems: From Theory to Algorithms*, NIC Series, edited by J. Grotendorst, D. Marx, and A. Muramatsu (John von Neumann Institute for Computing, Jülich, Germany, 2002), Vol. 10, pp. 467–506.
[11]A. Arnold and C. Holm, "Efficient methods to compute long-range interactions for soft matter systems," Adv. Polym. Sci. **185**, 59–109 (2005).
[12]T. A. Darden, "Extensions of the Ewald method for Coulomb interactions in crystals," in *International Tables for Crystallography: Volume B*, edited by U. Shmueli (International Union of Crystallography, 2010), Chap. 3.5, pp. 458–481.
[13]M. P. Allen and D. J. Tildesley, *Computer Simulations of Liquids*, 2nd ed. (Oxford University Press, Oxford, UK, 2017).
[14]T. Darden, D. York, and L. Pedersen, "Particle mesh Ewald: An $N \cdot \log(N)$ method for Ewald sums in large systems," J. Chem. Phys. **98**, 10089–10092 (1993).
[15]U. Essmann, L. Perera, M. L. Berkowitz, T. Darden, H. Lee, and L. G. Pedersen, "A smooth particle mesh Ewald method," J. Chem. Phys. **103**, 8577–8593 (1995).
[16]H. G. Petersen, "Accuracy and efficiency of the particle mesh Ewald method," J. Chem. Phys. **103**, 3668–3679 (1995).
[17]K. Nam, J. Gao, and D. M. York, "An efficient linear-scaling Ewald method for long-range electrostatic interactions in combined QM/MM calculations," J. Chem. Theory Comput. **1**, 2–13 (2005).
[18]D. Riccardi, P. Schaefer, and Q. Cui, "pK_a calculations in solution and proteins with QM/MM free energy perturbation simulations: A quantitative test of QM/MM protocols," J. Phys. Chem. B **109**, 17715–17733 (2005).
[19]R. C. Walker, M. F. Crowley, and D. A. Case, "The implementation of a fast and accurate QM/MM potential method in Amber," J. Comput. Chem. **29**, 1019–1031 (2008).
[20]K. Nam, "Acceleration of *ab initio* QM/MM calculations under periodic boundary conditions by multiscale and multiple time step approaches," J. Chem. Theory Comput. **10**, 4175–4183 (2014).
[21]Z. C. Holden, R. M. Richard, and J. M. Herbert, "Periodic boundary conditions for QM/MM calculations: Ewald summation for extended Gaussian basis sets," J. Chem. Phys. **139**, 244108, 1–13 (2013); Erratum, **142**, 059901 (2015).
[22]Z. C. Holden, "Long-range effects in QM/MM calculations: Ewald summation in non-minimal basis sets," Ph.D. thesis, Ohio State University, Columbus, OH, 2015).
[23]T. J. Giese and D. M. York, "Ambient-potential composite Ewald method for *ab initio* quantum mechanical/molecular mechanical molecular dynamics simulations," J. Chem. Theory Comput. **12**, 2611–2632 (2016).
[24]T. Vasilevskaya and W. Thiel, "Periodic boundary conditions in QM/MM calculations: Implementation and tests," J. Chem. Theory Comput. **12**, 3561–3570 (2016).
[25]C. M. Breneman and K. B. Wiberg, "Determining atom-centered monopoles from molecular electrostatic potentials. The need for high sampling density in formamide conformational analysis," J. Comput. Chem. **11**, 361–373 (1990).
[26]M. M. Francl and L. E. Chirlian, "The pluses and minuses of mapping atomic charges to electrostatic potentials," in *Reviews in Computational Chemistry*, edited by K. B. Lipkowitz and D. B. Boyd (Wiley VCH, New York, 2000), Vol. 14, Chap. 1, pp. 1–32.
[27]L. D. Jacobson and J. M. Herbert, "An efficient, fragment-based electronic structure method for molecular systems: Self-consistent polarization with perturbative two-body exchange and dispersion," J. Chem. Phys. **134**, 094118 (2011).
[28]J. M. Herbert, L. D. Jacobson, K. U. Lao, and M. A. Rohrdanz, "Rapid computation of intermolecular interactions in molecular and ionic clusters: Self-consistent polarization plus symmetry-adapted perturbation theory," Phys. Chem. Chem. Phys. **14**, 7679–7699 (2012).
[29]K. U. Lao and J. M. Herbert, "Accurate intermolecular interactions at dramatically reduced cost: XPol+SAPT with empirical dispersion," J. Phys. Chem. Lett. **3**, 3241–3248 (2012).
[30]L. D. Jacobson, R. M. Richard, K. U. Lao, and J. M. Herbert, "Efficient monomer-based quantum chemistry methods for molecular and ionic clusters," Annu. Rep. Comput. Chem. **9**, 25–56 (2013).
[31]K. U. Lao and J. M. Herbert, "An improved treatment of empirical dispersion and a many-body energy decomposition scheme for the explicit polarization plus symmetry-adapted perturbation theory (XSAPT) method," J. Chem. Phys. **139**, 034107 (2013); Erratum, **140**, 119901 (2014).
[32]R. M. Richard, K. U. Lao, and J. M. Herbert, "Aiming for benchmark accuracy with the many-body expansion," Acc. Chem. Res. **47**, 2828–2836 (2014).
[33]K. U. Lao and J. M. Herbert, "Accurate and efficient quantum chemistry calculations of non-covalent interactions in many-body systems: The XSAPT family of methods," J. Phys. Chem. A **119**, 235–253 (2015).
[34]K. U. Lao, K.-Y. Liu, R. M. Richard, and J. M. Herbert, "Understanding the many-body expansion for large systems. II. Accuracy considerations," J. Chem. Phys. **144**, 164105 (2016).
[35]K. U. Lao and J. M. Herbert, "Atomic orbital implementation of extended symmetry-adapted perturbation theory (XSAPT) and benchmark calculations for large supramolecular complexes," J. Chem. Theory Comput. **14**, 2955–2978 (2018).

Published under license by AIP Publishing

[36]J. M. Herbert and M. P. Coons, "The hydrated electron," Annu. Rev. Phys. Chem. **68**, 447–472 (2017).
[37]A. Mozumder, *Fundamentals of Radiation Chemistry* (Academic Press, San Diego, CA, 1999).
[38]M. Mostafavi and I. Lampre, "The solvated electron: A singular chemical species," in *Radiation Chemistry: From Basics to Applications in Material and Life Sciences*, edited by M. Spotheim-Maurizot, M. Mostafavi, J. Belloni, and T. Douki (EDP Sciences, 2008), Chap. 3, pp. 33–52.
[39]G. V. Buxton, "An overview of the radiation chemistry of liquids," in *Radiation Chemistry: From Basics to Applications in Material and Life Sciences*, edited by M. Spotheim-Maurizot, M. Mostafavi, J. Belloni, and T. Douki (EDP Sciences, 2008), Chap. 1, pp. 3–16.
[40]E. Alizadeh and L. Sanche, "Precursors of solvated electrons in radiobiological physics and chemistry," Chem. Rev. **112**, 5578–5602 (2012).
[41]Y. Gauduel, Y. Glinec, and V. Malka, "Femtoradical events in aqueous molecular environments: The tenuous borderline between direct and indirect radiation damages," J. Phys.: Conf. Ser. **101**, 012004 (2008).
[42]E. J. Hart and J. W. Boag, "Absorption spectrum of the hydrated electron in water and in aqueous solutions," J. Am. Chem. Soc. **84**, 4090–4095 (1962).
[43]E. J. Hart and J. W. Boag, "Absorption Spectra in Irradiated Water and Some Solutions: Absorption spectra of the 'hydrated' electron," Nature **197**, 45–47 (1963).
[44]E. J. Hart and M. Anbar, *The Hydrated Electron* (Wiley-Interscience, 1970).
[45]J. W. Boag, "Pulse radiolysis: A historical account of the discovery of the optical absorption spectrum of the hydrated electron," in *Early Developments in Radiation Chemistry*, edited by J. Kroh (Royal Society of Chemistry, Cambridge, UK, 1989), pp. 7–20.
[46]J. Jortner and S. A. Rice, "Theoretical studies of solvated electrons," in *Solvated Electron, Advances in Chemistry*, edited by R. F. Gould (American Chemical Society Publications, Washington, D.C., 1965), Vol. 50, Chap. 2, pp. 7–26.
[47]L. Kevan, "Solvated electron structure in glassy matrices," Acc. Chem. Res. **14**, 138–145 (1981).
[48]T. R. Tuttle, Jr. and S. Golden, "Solvated electrons: What is solvated?," J. Phys. Chem. **95**, 5725–5736 (1991).
[49]F. F. Muguet and G. W. Robinson, "Energetics and formation of the 'hydrated electron' within an itinerant radical model," AIP Conf. Proc. **298**, 158–170 (1994).
[50]A. L. Sobolewski and W. Domcke, "Hydrated hydronium: A cluster model of the solvated electron?," Phys. Chem. Chem. Phys. **4**, 4–10 (2002).
[51]L. Turi, M.-P. Gaigeot, N. Levy, and D. Borgis, "Analytical investigations of an electron–water molecule pseudopotential. I. Exact calculations on a model system," J. Chem. Phys. **114**, 7805–7815 (2001).
[52]L. Turi and Á. Madarász, "Comment on 'Does the hydrated electron occupy a cavity?,'" Science **331**, 1387 (2011).
[53]R. E. Larsen, W. J. Glover, and B. J. Schwartz, "Does the hydrated electron occupy a cavity?," Science **329**, 65–69 (2010).
[54]J. R. Casey, R. E. Larsen, and B. J. Schwartz, "Resonance Raman and temperature-dependent electronic absorption spectra of cavity and noncavity models of the hydrated electron," Proc. Natl. Acad. Sci. U. S. A. **110**, 2712–2717 (2013).
[55]J. R. Casey, A. Kahros, and B. J. Schwartz, "To be or not to be in a cavity: The hydrated electron dilemma," J. Phys. Chem. B **117**, 14173–14182 (2013).
[56]W. J. Glover and B. J. Schwartz, "Short-range electron correlation stabilizes noncavity solvation of the hydrated electron," J. Chem. Theory Comput. **12**, 5117–5131 (2016).
[57]C.-C. Zho and B. J. Schwartz, "Time-resolved photoelectron spectroscopy of the hydrated electron: Comparing cavity and noncavity models to experiment," J. Phys. Chem. B **120**, 12604–12614 (2016).
[58]C.-C. Zho, E. P. Farr, W. J. Glover, and B. J. Schwartz, "Temperature dependence of the hydrated electron's excited-state relaxation. I. Simulation predictions of resonance Raman and pump-probe transient absorption spectra of cavity and non-cavity models," J. Chem. Phys. **147**, 074503 (2017).
[59]L. D. Jacobson and J. M. Herbert, "Comment on 'Does the hydrated electron occupy a cavity?,'" Science **331**, 1387 (2011).
[60]R. E. Larsen, W. J. Glover, and B. J. Schwartz, "Response to comment on 'Does the hydrated electron occupy a cavity?,'" Science **331**, 1387 (2011).
[61]J. M. Herbert and L. D. Jacobson, "Structure of the aqueous electron: Assessment of one-electron pseudopotential models in comparison to experimental data and time-dependent density functional theory," J. Phys. Chem. A **115**, 14470–14483 (2011).
[62]M. Boero, M. Parrinello, K. Terakura, T. Ikeshoji, and C. C. Liew, "First-principles molecular-dynamics simulations of a hydrated electron in normal and supercritical water," Phys. Rev. Lett. **90**, 226403 (2003).
[63]M. Boero, "Excess electron in water at different thermodynamic conditions," J. Phys. Chem. A **111**, 12248–12256 (2007).
[64]F. Uhlig, O. Marsalek, and P. Jungwirth, "Unraveling the complex nature of the hydrated electron," J. Phys. Chem. Lett. **3**, 3071–3075 (2012); Erratum, **4**, 603 (2013).
[65]O. Marsalek, F. Uhlig, J. VandeVondele, and P. Jungwirth, "Structure, dynamics, and reactivity of hydrated electrons by *ab initio* molecular dynamics," Acc. Chem. Res. **45**, 23–32 (2012).
[66]F. Ambrosio, G. Miceli, and A. Pasquarello, "Electronic levels of excess electrons in liquid water," J. Phys. Chem. Lett. **8**, 2055–2059 (2017).
[67]M.-C. Kim, E. Sim, and K. Burke, "Communication: Avoiding unbound anions in density functional calculations," J. Chem. Phys. **134**, 171103 (2011).
[68]J. M. Herbert, "The quantum chemistry of loosely bound electrons," in *Reviews in Computational Chemistry*, edited by A. L. Parill and K. Lipkowitz (Wiley VCH, 2015), Vol. 28, Chap. 8, pp. 391–517.
[69]J. VandeVondele and M. Sprik, "A molecular dynamics study of the hydroxyl radical in solution applying self-interaction-corrected density functional methods," Phys. Chem. Chem. Phys. **7**, 1363–1367 (2005).
[70]M.-C. Kim, E. Sim, and K. Burke, "Ions in solution: Density corrected density functional theory (DC-DFT)," J. Chem. Phys. **140**, 18A528 (2014).
[71]S. Bogusz, T. E. Cheatham III, and B. R. Brooks, "Removal of pressure and free energy artifacts in charged periodic systems via net charge corrections to the Ewald potential," J. Chem. Phys. **108**, 7070–7084 (1998).
[72]D. J. Adams and G. S. Dubey, "Taming the Ewald sum in the computer simulation of charged systems," J. Comput. Phys. **72**, 156–176 (1987).
[73]D. Frenkel and B. Smit, *Understanding Molecular Simulation: From Algorithms to Applications* (Academic Press, San Diego, 2002).
[74]B. Stamm, L. Lagardère, É. Polack, Y. Maday, and J.-P. Piquemal, "A coherent derivation of the Ewald summation for arbitrary orders of multipoles: The self-terms," J. Chem. Phys. **149**, 124103 (2018).
[75]J. S. Hub, B. L. de Groot, H. Grubmüller, and G. Groenhof, "Quantifying artifacts in Ewald simulations of inhomogeneous systems with a net charge," J. Chem. Theory Comput. **10**, 381–390 (2014).
[76]F. Figueirido, G. S. Del Buono, and R. M. Levy, "On finite-size effects in computer simulations using the Ewald potential," J. Chem. Phys. **103**, 6133–6142 (1995).
[77]V. Ballenegger, A. Arnold, and J. J. Cerdà, "Simulations of non-neutral slab systems with long-range electrostatic interactions in two-dimensional periodic boundary conditions," J. Chem. Phys. **131**, 094107 (2009).
[78]G. Hummer, N. Grønbech-Jensen, and M. Neumann, "Pressure calculation in polar and charged systems using Ewald summation: Results for the extended simple point charge model of water," J. Chem. Phys. **109**, 2791–2797 (1998).
[79]J. Stenhammar, M. Trulsson, and P. Linse, "Some comments and corrections regarding the calculation of electrostatic potential derivatives using the Ewald summation technique," J. Chem. Phys. **134**, 224101 (2011).
[80]V. Ballenegger, "Communication: On the origin of the surface term in the Ewald formula," J. Chem. Phys. **140**, 161102 (2014).
[81]J. A. Pople, R. Krishnan, H. B. Schlegel, and J. S. Binkley, "Derivative studies in Hartree–Fock and Møller–Plesset theories," Int. J. Quantum Chem. **13**, 225–241 (1979); available at http://www.chem.wayne.edu/schlegel/Pub_folder/32.pdf.
[82]Y. Yamaguchi, Y. Osamura, J. D. Goddard, and H. F. Schaefer III, *A New Dimension to Quantum Chemistry: Analytic Derivative Methods in Ab Initio Molecular Electronic Structure Theory* (Oxford University Press, New York, 1994).

Published under license by AIP Publishing

[83]T. R. Stouch and D. E. Williams, "Conformational dependence of electrostatic potential-derived charges: Studies of the fitting procedure," J. Comput. Chem. **14**, 858–866 (1993).
[84]M. M. Francl, C. Carey, L. E. Chirlian, and D. M. Gange, "Charges fit to electrostatic potentials. II. Can atomic charges be unambiguously fit to electrostatic potentials?," J. Comput. Chem. **17**, 367–383 (1996).
[85]A. W. Lange and J. M. Herbert, "Polarizable continuum reaction-field solvation models affording smooth potential energy surfaces," J. Phys. Chem. Lett. **1**, 556–561 (2010).
[86]A. W. Lange and J. M. Herbert, "A smooth, non-singular, and faithful discretization scheme for polarizable continuum models: The switching/Gaussian approach," J. Chem. Phys. **133**, 244111 (2010).
[87]Y. Shao, Z. Gan, E. Epifanovsky, A. T. B. Gilbert, M. Wormit, J. Kussmann, A. W. Lange, A. Behn, J. Deng, X. Feng, D. Ghosh, M. Goldey, P. R. Horn, L. D. Jacobson, I. Kaliman, R. Z. Khaliullin, T. Kús, A. Landau, J. Liu, E. I. Proynov, Y. M. Rhee, R. M. Richard, M. A. Rohrdanz, R. P. Steele, E. J. Sundstrom, H. L. Woodcock III, P. M. Zimmerman, D. Zuev, B. Albrecht, E. Alguire, B. Austin, G. J. O. Beran, Y. A. Bernard, E. Berquist, K. Brandhorst, K. B. Bravaya, S. T. Brown, D. Casanova, C.-M. Chang, Y. Chen, S. H. Chien, K. D. Closser, D. L. Crittenden, M. Diedenhofen, R. A. H. DiStasio Do, Jr., A. D. Dutoi, R. G. Edgar, S. Fatehi, L. Fusti-Molnar, A. Ghysels, A. Golubeva-Zadorozhnaya, J. Gomes, M. W. D. Hanson-Heine, P. H. P. Harbach, A. W. Hauser, E. G. Hohenstein, Z. C. Holden, T.-C. Jagau, H. Ji, B. Kaduk, K. Khistyaev, J. Kim, J. Kim, R. A. King, P. Klunzinger, D. Kosenkov, T. Kowalczyk, C. M. Krauter, K. U. Lao, A. Laurent, K. V. Lawler, S. V. Levchenko, C. Y. Lin, F. Liu, E. Livshits, R. C. Lochan, A. Luenser, P. Manohar, S. F. Manzer, S.-P. Mao, N. Mardirossian, A. V. Marenich, S. A. Maurer, N. J. Mayhall, C. M. Oana, R. Olivares-Amaya, D. P. O'Neill, J. A. Parkhill, T. M. Perrine, R. Peverati, P. A. Pieniazek, A. Prociuk, D. R. Rehn, E. Rosta, N. J. Russ, N. Sergueev, S. M. Sharada, S. Sharma, D. W. Small, A. Sodt, T. Stein, D. Stück, Y.-C. Su, A. J. W. Thom, T. Tsuchimochi, L. Vogt, O. Vydrov, T. Wang, M. A. Watson, J. Wenzel, A. White, C. F. Williams, V. Vanovschi, S. Yeganeh, S. R. Yost, Z.-Q. You, I. Y. Zhang, X. Zhang, Y. Zhao, B. R. Brooks, G. K. L. Chan, D. M. Chipman, C. J. Cramer, W. A. M. S. GoddardGordon III, W. J. Hehre, A. Klamt, H. F. Schaefer III, M. W. Schmidt, C. D. Sherrill, D. G. Truhlar, A. Warshel, X. Xu, A. Aspuru-Guzik, R. Baer, A. T. Bell, N. A. Besley, J.-D. Chai, A. Dreuw, B. D. Dunietz, T. R. Furlani, S. R. Gwaltney, C.-P. Hsu, Y. Jung, J. Kong, D. S. Lambrecht, W. Liang, C. Ochsenfeld, V. A. Rassolov, L. V. Slipchenko, J. E. Subotnik, T. Van Voorhis, J. M. Herbert, A. I. Krylov, P. M. W. Gill, and M. Head-Gordon, "Advances in molecular quantum chemistry contained in the Q-Chem 4 program package," Mol. Phys. **113**, 184–215 (2015).
[88]B. R. Brooks, C. L. Brooks III, A. D. Mackerell, Jr., L. Nilsson, R. J. Petrella, B. Roux, Y. Won, G. Archontis, C. Bartels, S. Boresch, A. Caflisch, L. Caves, C. Qui, A. R. Dinner, M. Feig, S. Fischer, J. Gao, M. Hodoscek, W. Im, K. Kuczera, T. Lazaridis, J. Ma, V. Ovchinnikov, E. Paci, R. W. Pastor, C. B. Post, J. Z. Pu, M. Schaefer, B. Tidor, R. M. Venable, H. L. Woodcock, X. Wu, W. Yang, D. M. York, and M. Karplus, "CHARMM: The biomolecular simulation program," J. Comput. Chem. **30**, 1545–1614 (2009).
[89]L. D. Jacobson and J. M. Herbert, "A one-electron model for the aqueous electron that includes many-body electron-water polarization: Bulk equilibrium structure, vertical electron binding energy, and optical absorption spectrum," J. Chem. Phys. **133**, 154506 (2010).
[90]M. P. Coons, Z.-Q. You, and J. M. Herbert, "The hydrated electron at the surface of neat liquid water appears to be indistinguishable from the bulk species," J. Am. Chem. Soc. **138**, 10879–10886 (2016).
[91]G. Hummer, L. R. Pratt, and A. E. García, "Free energy of ionic hydration," J. Phys. Chem. **100**, 1206–1215 (1996).
[92]G. Hummer, L. R. Pratt, and A. E. García, "Ion sizes and finite-size corrections for ionic-solvation free energies," J. Chem. Phys. **107**, 9275–9277 (1997).
[93]S. Sakane, H. S. Ashbaugh, and R. H. Wood, "Continuum corrections to the polarization and thermodynamic properties of Ewald sum simulations for ions and ion pairs at infinite dilution," J. Phys. Chem. B **102**, 5673–5682 (1998).
[94]P. H. Hünenberger and J. A. McCammon, "Effect of artificial periodicity in simulations of biomolecules under Ewald boundary conditions: A continuum electrostatics study," Biophys. Chem. **78**, 69–88 (1999).
[95]G. J. Rocklin, D. L. Mobley, K. A. Dill, and P. H. Hünenberger, "Calculating the binding free energies of charged species based on explicit-solvent simulations employing lattice-sum methods: An accurate correction scheme for electrostatic finite-size effects," J. Chem. Phys. **139**, 184103 (2013).
[96]Y.-L. Lin, A. Aleksandrov, T. Simonson, and B. Roux, "An overview of electrostatic free energy computations for solutions and proteins," J. Chem. Theory Comput. **10**, 2690–2709 (2014).
[97]T. Simonson and B. Roux, "Concepts and protocols for electrostatic free energies," Mol. Simul. **42**, 1090–1101 (2016).
[98]S. Boresch and O. Steinhauser, "Presumed versus real artifacts of the Ewald summation technique: The importance of dielectric boundary conditions," Ber. Bunsengesellschaft Phys. Chem. **101**, 1019–1029 (1997).
[99]M. P. Coons and J. M. Herbert, "Quantum chemistry in arbitrary dielectric environments: Theory and implementation of nonequilibrium Poisson boundary conditions and application to compute vertical ionization energies at the air/water interface," J. Chem. Phys. **148**, 222834 (2018).
[100]J. Schnitker and P. J. Rossky, "Quantum simulation study of the hydrated electron," J. Chem. Phys. **86**, 3471–3485 (1987).
[101]L. Turi and D. Borgis, "Analytical investigations of an electron–water molecule pseudopotential. II. Development of a new pair potential and molecular dynamics simulations," J. Chem. Phys. **117**, 6186–6195 (2002).
[102]G. A. Kenney-Wallace and C. D. Jonah, "Picosecond spectroscopy and solvation clusters. The dynamics of localizing electrons in polar fluids," J. Phys. Chem. **86**, 2572–2586 (1982).
[103]A. Migus, Y. Gauduel, J. L. Martin, and A. Antonetti, "Excess electrons in liquid water: First evidence of a prehydrated state with femtosecond lifetime," Phys. Rev. Lett. **58**, 1559–1562 (1987).
[104]J. Savolainen, F. Uhlig, S. Ahmed, P. Hamm, and P. Jungwirth, "Direct observation of the collapse of the delocalized excess electron in water," Nat. Phys. **6**, 697–701 (2014).
[105]A. D. Mackerell, Jr., D. Bashford, M. Bellott, R. L. Dunbrack, Jr., J. D. Evanseck, M. J. Field, S. Fischer, J. Gao, H. Guo, S. Ha, D. Joseph-McCarthy, L. Kuchnir, K. Kuczera, F. T. K. Lau, C. Mattos, S. Michnick, T. Ngo, D. T. Nguyen, B. Prodhom, W. E. Reiher III, B. Roux, M. Schlenkrich, J. C. Smith, R. Stote, J. Straub, M. Wantanabe, J. Wiórkiewicz-Kuczera, D. Yin, and M. Karplus, "All-atom empirical potential for molecular modeling and dynamics studies of proteins," J. Phys. Chem. B **102**, 3586–3616 (1998).
[106]M. Freindorf and J. Gao, "Optimization of the Lennard-Jones parameters for a combined *ab initio* quantum mechanical and molecular mechanical potential using the 3-21G basis set," J. Comput. Chem. **17**, 386–395 (1996).
[107]M. Freindorf, Y. Shao, T. R. Furlani, and J. Kong, "Lennard-Jones parameters for the combined QM/MM method using the B3LYP/6-31G*/AMBER potential," J. Comput. Chem. **26**, 1270–1278 (2005).
[108]E. R. Kuechler, T. J. Giese, and D. M. York, "Charge-dependent many-body exchange and dispersion interactions in combined QM/MM simulations," J. Chem. Phys. **143**, 234111 (2015).
[109]S. Grimme, J. Antony, S. Ehrlich, and H. Krieg, ""A consistent and accurate *ab initio* parameterization of density functional dispersion correction (DFT-D) for the 94 elements H–Pu," J. Chem. Phys. **132**, 154104 (2010).
[110]J. M. Herbert and M. Head-Gordon, "Accelerated, energy-conserving Born-Oppenheimer molecular dynamics *via* Fock matrix extrapolation," Phys. Chem. Chem. Phys. **7**, 3269–3275 (2005).
[111]L. D. Jacobson and J. M. Herbert, "Polarization-bound quasi-continuum states are responsible for the 'blue tail' in the optical absorption spectrum of the aqueous electron," J. Am. Chem. Soc. **132**, 10000–10002 (2010).
[112]J. M. Herbert and M. Head-Gordon, "Calculation of electron detachment energies for water cluster anions: An appraisal of electronic structure methods, with application to $(H_2O)_{20}^-$ and $(H_2O)_{24}^-$," J. Phys. Chem. A **109**, 5217–5229 (2005).
[113]J. Gao, D. G. Truhlar, Y. Wang, M. J. M. Mazack, P. Löffler, M. R. Provorse, and P. Rehak, "Explicit polarization: A quantum mechanical framework for developing next generation force fields," Acc. Chem. Res. **47**, 2837–2845 (2014).
[114]Y. Wang, M. J. M. Mazack, D. G. Truhlar, and J. Gao, "Explicit polarization theory," in *Many-Body Effects and Electrostatics in Biomolecules*, edited by Q. Cui, M. Meuwly, and P. Ren (Pan Stanford, Boca Raton, FL, 2016), Chap. 2, pp. 33–64.
[115]S. Koneshan, J. C. Rasaiah, R. M. Lynden-Bell, and S. H. Lee, "Solvent structure, dynamics, and ion mobility in aqueous solutions at 25 °C," J. Phys. Chem. B **102**, 4193–4204 (1998).

Published under license by AIP Publishing

[116]J. M. Heuft and E. J. Meijer, "Density functional theory based molecular-dynamics study of aqueous iodide solvation," J. Chem. Phys. **123**, 094506 (2005).
[117]J. Boisson, G. Stirnemann, D. Laage, and J. T. Hynes, "Water reorientation dynamics in the first hydration shells of F^- and I^-," Phys. Chem. Chem. Phys. **13**, 19895–19901 (2011).
[118]A. Karmakar and A. Chandra, "Water in hydration shell of an iodide ion: Structure and dynamics of solute-water hydrogen bonds and vibrational spectral diffusion from first-principles simulations," J. Phys. Chem. B **119**, 8561–8572 (2015).
[119]A. W. Duster, C.-H. Wang, C. M. Garza, D. E. Miller, and H. Lin, "Adaptive quantum/molecular mechanics: What have we learned, where are we, and where do we go from here?," Wiley Interdiscip. Rev.: Comput. Mol. Sci. **7**, e1310 (2017).
[120]C. N. Rowley and B. Roux, "The solvation structure of Na^+ and K^+ in liquid water determined from high level *ab initio* molecular dynamics simulations," J. Chem. Theory Comput. **8**, 3526–3535 (2012).
[121]D. Marx and J. Hutter, *Ab Initio Molecular Dynamics: Basic Theory and Advanced Methods* (Cambridge University Press, Cambridge, UK, 2009).
[122]R. P. Steele, "Multiple-timestep *ab initio* molecular dynamics using an atomic basis set partitioning," J. Phys. Chem. A **119**, 12119–12130 (2015).
[123]J. D. Herr and R. P. Steele, "Accelerating *ab initio* molecular dynamics simulations by linear prediction methods," Chem. Phys. Lett. **661**, 42–47 (2016).
[124]P. H. Hünenberger, "Thermostat algorithms for molecular dynamics simulations," Adv. Polym. Sci. **173**, 105–149 (2005).
[125]M. J. Tauber and R. A. Mathies, "Structure of the aqueous solvated electron from resonance Raman spectroscopy: Lessons from isotopic mixtures," J. Am. Chem. Soc. **125**, 1394–1402 (2003).
[126]C. F. Williams and J. M. Herbert, "Influence of structure on electron correlation effects and electron–water dispersion interactions in anionic water clusters," J. Phys. Chem. A **112**, 6171–6178 (2008).
[127]J. M. Herbert and L. D. Jacobson, "Nature's most squishy ion: The important role of solvent polarization in the description of the hydrated electron," Int. Rev. Phys. Chem. **30**, 1–48 (2011).
[128]J. Simons, "Molecular anions," J. Phys. Chem. A **112**, 6401–6511 (2008).
[129]D. Luckhaus, Y. Yamamoto, T. Suzuki, and R. Signorell, "Genuine binding energy of the hydrated electron," Sci. Adv. **3**, e1603224 (2017).
[130]C. J. Smallwood, R. E. Larsen, W. J. Glover, and B. J. Schwartz, "A computationally efficient exact pseudopotential method. I. Analytic reformulation of the Phillips-Kleinman theory," J. Chem. Phys. **125**, 074102 (2006).
[131]L. D. Jacobson, C. F. Williams, and J. M. Herbert, "The static-exchange electron-water pseudopotential, in conjunction with a polarizable water model: A new Hamiltonian for hydrated-electron simulations," J. Chem. Phys. **130**, 124115 (2009).
[132]L. Turi, "Hydrated electrons in water clusters: Inside or outside, cavity or noncavity?," J. Chem. Theory Comput. **11**, 1745–1755 (2015).
[133]D. C. Walker, "Dynamics of electron localization," J. Phys. Chem. **84**, 1140–1144 (1980).
[134]D. Huppert, G. A. Kenney-Wallace, and P. M. Rentzepis, "Picosecond infrared dynamics of electron trapping in polar liquids," J. Chem. Phys. **75**, 2265–2269 (1981).
[135]A. Mozumder, "Conjecture on electron trapping in liquid water," Radiat. Phys. Chem. **32**, 287–291 (1988).
[136]M. Hilczer, W. M. Bartczak, and M. Sopek, "Electron localization in liquid alcohols. A statistical model," Radiat. Phys. Chem. **36**, 199–202 (1990).
[137]W. M. Bartczak and K. Pernal, "Potential traps for an excess electron in liquid water. Geometry, energy distributions and lifetime," Comput. Chem. **24**, 469–482 (2000).
[138]J. Schnitker, P. J. Rossky, and G. A. Kenney-Wallace, "Electron localization in liquid water: A computer simulation study of microscopic trapping sites," J. Chem. Phys. **85**, 2986–2998 (1986).
[139]D. Nordlund, H. Ogasawara, H. Bluhm, O. Takahashi, M. Odelius, M. Nagasono, L. G. M. Pettersson, and A. Nilsson, "Probing the electron delocalization in liquid water and ice at attosecond time scales," Phys. Rev. Lett. **99**, 217406 (2007).
[140]F. H. Long, H. Lu, and K. B. Eisenthal, "Femtosecond studies of the presolvated electron: An excited state of the solvated electron?," Phys. Rev. Lett. **64**, 1469–1472 (1990).
[141]X. Shi, F. H. Long, H. Lu, and K. B. Eisenthal, "Femtosecond electron solvation kinetics in water," J. Phys. Chem. **100**, 11903–11906 (1996).
[142]R. Laenen, T. Roth, and A. Laubereau, "Novel precursors of solvated electrons in water: Evidence for a charge transfer process," Phys. Rev. Lett. **85**, 50–53 (2000).
[143]P. Kambhampati, D. H. Son, T. W. Kee, and P. F. Barbara, "Solvation dynamics of the hydrated electron depends on its initial degree of electron delocalization," J. Phys. Chem. A **106**, 2374–2378 (2002).
[144]C.-R. Wang, T. Luo, and Q.-B. Lu, "On the lifetimes and physical nature of incompletely relaxed electrons in liquid water," Phys. Chem. Chem. Phys. **10**, 4463–4470 (2008).
[145]H. Iglev, S. K. Kolev, H. Rossmadl, P. S. Petkov, and G. N. Vayssilov, "Hydrogen atom transfer from water or alcohols activated by presolvated electrons," J. Phys. Chem. Lett. **6**, 986–992 (2015).
[146]J. Ma, F. Wang, S. A. Denisov, A. Adhikary, and M. Mostafavi, "Reactivity of prehydrated electrons toward nucleobases and nucleotides in aqueous solution," Sci. Adv. **3**, e1701669 (2017).
[147]J. Wilhelm, J. VandeVondele, and V. V. Rybkin, "Dynamics of the bulk hydrated electron from many-body wave-function theory," Angew. Chem. Int. Ed. Engl. **58**, 3890–3893 (2019).
[148]H. L. Woodcock III, M. Hodošček, A. T. B. Gilbert, P. M. W. Gill, H. F. Schaefer III, and B. R. Brooks, "Interfacing Q-Chem and CHARMM to perform QM/MM reaction path calculations," J. Comput. Chem. **28**, 1485–1502 (2007).
[149]See http://osc.edu/ark:/19495/f5s1ph73 for Ohio Supercomputer Center.

Published under license by AIP Publishing